CHALMERS
UNIVERSITY OF TECHNOLOGY

Optimization Under Uncertainty in Industrial Energy Systems

A Robust Optimization Framework

Master's thesis in Innovative Sustainable Energy Engineering

ARTHUR VANKEIRSBILCK

Master's thesis in Space, Earth and Environment

CHALMERS UNIVERSITY OF TECHNOLOGY
Gothenburg, Sweden 2024
www.chalmers.se

Master's thesis 2024

Optimization Under Uncertainty in Industrial Energy Systems

A Robust Optimization Framework

ARTHUR VANKEIRSBILCK

CHALMERS
UNIVERSITY OF TECHNOLOGY

Master's thesis in Space, Earth and Environment
Division of Energy Technology
Chalmers University of Technology
Gothenburg, Sweden 2024

Optimization Under Uncertainty in Industrial Energy Systems
A Robust Optimization Framework
ARTHUR VANKEIRSBILCK

Supervisor: Prof. François Maréchal, École Polytechnique Fédérale de Lausanne, Industrial Process and Energy Systems Engineering lab
Examiner: Prof. Simon Harvey, Chalmers University of Technology, Department of Energy Technology

Master's Thesis 2024
Department of Energy Technology
Division Space, Earth and Environment
Chalmers University of Technology
SE-412 96 Gothenburg
Telephone +46 31 772 1000

Typeset in LaTeX
Printed by Chalmers Reproservice
Gothenburg, Sweden 2024

Optimization Under Uncertainty in Industrial Energy Systems
A Robust Optimization Framework
ARTHUR VANKEIRSBILCK
Department of Energy Technology
Chalmers University of Technology

Abstract

The growing global demand for improved energy efficiency in the process industries, which are significant consumers of both fuels and raw materials, necessitates advanced optimization strategies. This thesis presents a robust optimization framework aimed at enhancing the efficiency and sustainability of industrial energy systems under uncertainty. The framework employs Mixed-Integer Linear Programming to model and optimize energy and mass transfer within industrial clusters, considering the volatility of energy prices.

The methodology integrates a set-induced robust optimization reformulation to ensure solutions remain feasible and optimal under uncertainty. This approach contrasts with traditional sensitivity analysis and stochastic programming by focusing on the worst-case scenario within predefined uncertainty bounds, thus providing a reliable decision-making tool for planners and operators in the energy sector.

Key components of the study include the development of base case models for existing technologies such as natural gas boilers, cogeneration units, and absorption chillers, as well as models for decarbonization technologies like biomass-fired boilers, amine CO_2 capture, and high-temperature electrolysis. The framework's application demonstrates significant potential for optimizing energy consumption and reducing emissions in industrial clusters.

The results underscore the importance of robust optimization in managing uncertainties, facilitating informed decisions that enhance the sustainability and efficiency of resource use. This research contributes to the broader field of industrial energy system optimization, offering a robust and practical solution to the challenges posed by fluctuating variables and the integration of renewable energy sources.

Keywords: Decarbonization, Energy Efficiency, Industrial Energy Systems, Mixed-Integer Linear Programming, Robust Optimization, Uncertainty Management.

Acknowledgements

I am deeply grateful for the support and guidance I have received throughout the course of this research. First, I would like to express my sincere gratitude to my supervisors, Francois Marechal, Simon Harvey and Risto Lahdelma, whose expertise added considerably to my graduate experience. Your willingness to give your time so generously has been greatly appreciated.
I am also thankful to École polytechnique fédérale de Lausanne for providing the necessary funding/support needed to conduct this research.
I must acknowledge my peers at École polytechnique fédérale de Lausanne, Shivom Sharma, Lorenzo Aimone and Daniel Flórez-Orrego, for all the thoughtful discussions and for the stimulating environment that they provided.
My heartfelt thanks also go to my family and friends, who have supported me immensely throughout this journey both emotionally and intellectually.

Arthur Vankeirsbilck, Sion Switzerland, June 2024

List of Acronyms

Below is the list of acronyms that have been used throughout this thesis listed in alphabetical order:

CAPEX	Capital Expenditure
CC	Carbon Capture
CHP	Combined Heat and Power
COP	Coefficient of Performance
GCC	Grand-Composite Curve
KPI	Key Performance Indicator
MILP	Mixed-Integer Linear Programming
PEM	Polymer Electrolyte Membrane
OF	Objective Function
OPEX	Operational Expenditure
SOEC	Solid Oxide Electrochemical Cell
RC	Robust Counterpart
RO	Robust Optimization
SNG	Synthetic Natural Gas
TOTEX	Total Expenditure

Contents

List of Figures

List of Tables

1

Introduction

The growing demand for improved energy efficiency is a global concern, and is particularly pressing in the process industries, which are major consumers of energy, both in the form of fuels and raw materials [Eurostat, 2024]. These industries, often organised into 'clusters', comprise a wide range of stakeholders, including utilities and various production companies. Each company operates with different objectives and seeks to invest according to individual criteria. By taking a comprehensive view of these clusters, bringing together different industries within a single, coherent framework, the potential for optimising energy sources across sectors is greatly enhanced [Parekh et al., 2023, Bhuiyan et al., 2022]. This integrated approach aims not only to reduce waste - be it waste in the form of heat, industrial by-products or waste water - but also to promote a culture of sustainable and efficient resource use.

The identification and definition of opportunities for improvement in the process industries, particularly through the use of modelling, can be challenging. Some of these challenges include data issues such as the scarcity of data, which is often incomplete or prone to inaccuracies. In addition, uncertainty is emerging as a dominant factor affecting both the planning and operational phases of industry operations. In particular, the planning phase faces significant uncertainty, which is made more difficult by the increasing integration of variable energy sources and the use of distributed energy resources. This reality manifests itself in the form of volatile energy costs, adding a layer of complexity to the decision-making process.

In today's dynamic and ever-changing industrial energy landscape, the complexity of variables that need to be considered when developing effective solutions has increased significantly. This complexity is due to a number of factors, including the emergence of renewable energy sources that are characterised by intermittent output. This variability requires a delicate balance between the installed capacity of renewable energy source, the need for energy storage systems, the capacity to provide back-up energy during periods of unavailability or high prices. In addition, the introduction of new technologies and different energy resources such as hydrogen, methanol, synthetic natural gas, referred to here as energy vectors has led to a more interconnected energy landscape. Examples include hydrogen, which can be produced from electricity or natural gas, and synthetic fuels such as methanol, synthethic natural gas (SNG), biofuels. These advances complicate the process of selecting the most appropriate technical solutions and determining the optimal scale of new installations.

In order to deal with these uncertainties and to effectively navigate through the complexities of fluctuating variables, advanced data analysis and modelling frameworks are required. This thesis explores a general framework for optimising heat

and mass transfer in industrial clusters, using a Mixed-Integer Linear Programming (MILP) approach. The framework incorporates a uncertainty set induced robust optimization reformulation to manage uncertainty, with the aim of developing robust solutions capable of adapting to variations in energy costs. As a result, this methodological approach provides decision makers with a tool equipped to make informed decisions and enhances both the sustainability and efficiency of resource use under prevailing uncertainties.

Optimisation techniques are at the forefront of efforts to improve efficiency and planning in process industries [Acevedo and Pistikopoulos, 1998, Shi and You, 2016, Ye et al., 2014]. They are central to the management of essential resources such as energy and water within industrial clusters. These resources are not only vital to the economic viability of these industries, but also have a profound impact on their environmental footprint. The drive to develop optimisation methods stems from the urgent need to address complex resource planning and management issues amidst the diverse operational requirements of industrial activities. In addition to cost savings, these methods are critical to reducing energy and water consumption in response to escalating fuel costs, the need to reduce carbon emissions and the need to conserve water.

The emergence of optimisation in the process industries marks a significant advance in computational methods and demonstrates a strong commitment to sustainability. The application of these optimisation techniques has led to significant improvements in efficiency, economy and environmental protection, underlining their importance in the modern industrial framework. This introduction sets the stage for a thorough exploration of optimisation in the process industries, highlighting the intricate dynamics and significant impact of these strategies in a sector navigating the complexities of multi-energy industrial cluster optimisation and the uncertainties involved.

1.1 Research Gap and Questions

Despite significant advances in optimization frameworks for industrial energy systems, several limitations persist in the existing body of research. These gaps provide an opportunity for further investigation to enhance the efficiency and sustainability of such systems under uncertainty.

Limitations of Previous Studies

Many existing studies have not adequately addressed the uncertainty inherent in energy prices and demand. This gap limits the practical applicability of their optimization models in real-world scenarios [Sun et al., 2018, Mitra and Grossmann, 2019]. Additionally, previous research often lacks comprehensive integration of various decarbonization technologies within industrial clusters, which is essential for achieving significant CO_2 reductions [Chen and Zhang, 2020, Zhang and Li, 2017]. There is also a scarcity of studies that compare the outcomes of robust optimization

approaches with mean value-based methods, particularly in the context of operational and investment costs [Guo and Huang, 2021, Li and Fan, 2018]. Furthermore, many optimization models proposed in earlier research struggle with scalability when applied to large and complex industrial systems, limiting their usefulness for broader industrial applications [He and Li, 2019, Liu and Zhang, 2020].

1. *How can robust optimization frameworks be applied and developed to enhance the efficiency and sustainability of industrial energy systems under uncertainty?*

   This question explores the development and application of robust optimization frameworks, specifically utilizing Mixed-Integer Linear Programming (MILP) to model and optimize energy and mass transfer within industrial clusters and considers the volatility of energy prices and investigates deterministic reformulations of robust optimization formulations.

2. *What are the impacts of different CO_2 reduction scenarios under uncertainty on the operational and investment costs in industrial clusters and what are the differences between robust and mean formulations?*

   This question investigates the effects of various CO_2 reduction strategies on both the OPEX and CAPEX within industrial clusters. It includes the integration and optimization of decarbonization technologies developed in this work, and examines the differences between robust and mean formulations.

2
Theory

This chapter outlines the optimization methodology and formulations employed in this thesis. Section 2.1.3 introduces the foundational principles and mathematical formulations of the optimization problems addressed in this research, serving as the basis for understanding the structure of optimization objectives and constraints. Following this, Sections 2.2.1 to 2.2.3 discuss the rationale behind utilizing a RO framework. The robust framework is chosen to effectively handle uncertainties in model parameters, ensuring that solutions remain feasible and optimal under various scenarios. This discussion includes a comparative analysis with stochastic and other optimization methods.
In Sections 2.2.4 to 2.2.4.2, the theoretical aspects of Robust Optimization (RO) are explored in detail. These sections provide a comprehensive description of RO techniques, including the formulation of uncertainty sets and the transformation of the original optimization problems into their Robust Counterparts (RCs).
Furthermore, the approach for modeling heat, as discussed in Section 2.3, and steam energy, covered in Section 2.4, is decoupled from the mass balance equations in all developed technology models. This decoupling facilitates a more flexible and accurate representation of energy and heat flows within the optimization framework.

2.1 Optimization Framework

The methodology used in this work is Multi-Objective Optimization of Integrated Energy Systems (OSMOSE) [Maréchal and Kalitventzeff, 1998, Kermani et al., 2017, Kermani, Maziar, 2018]. The aim of this methodology is to optimize an industrial site according to one or more user-defined criteria. To do this, different technical solutions are analyzed, and only the best configuration, which optimizes the defined criterions while respecting the site's operating constraints, is selected. To carry out this optimization study, it is necessary to develop a model of an industrial site, characterizing interactions (with external consumers, networks, etc.), processes, utility production resources and operating constraints.
The optimization process implemented within the optimization model is illustrated in Figure 2.1. The superstructure, comprising process models and economic data, is fed with input data typically characterizing the operating points to be studied. This set of models and data is then converted into a linear optimization problem. Once the model has been solved, the results obtained are post-processed to obtain relevant information such as key performance indicators (KPIs) and, for example, operating patterns by time operating points.

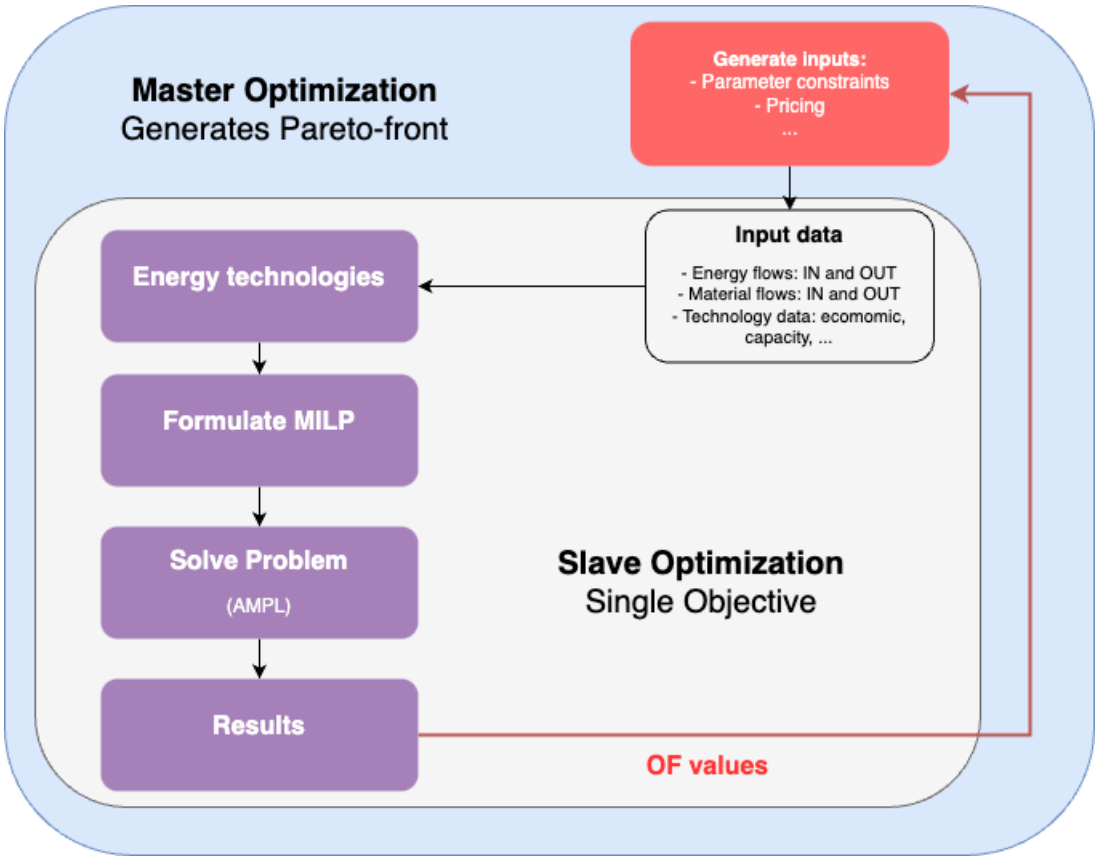

Figure 2.1: Optimization process within the framework, case of a single-objective optimization.

2.1.1 Superstructure development

The modeling approach adopted in this study is both technical and economic. A model for each of the industrial units is developed and connected to the site's other units via material, energy and heat flows. Thus, for each of the units making up the industrial site, material, energy (excluding heat) and heat flows are defined as inputs and outputs. Each unit is also defined in terms of operating costs and investment costs. These elements (material, energy and thermal flows, economic data) are derived from:

- Modelling using software such as ProSimPlus or Aspen Plus;
- Fluid properties from Coolprop;
- Literature;
- Technology supplier datasheets.

In addition, because of the linear nature of the optimization problem, which requires acceptable costs and solution times compatible with the study of complex industrial systems, the relationships between unit capacity, input and/or output quantities must be linear, and operating and/or investment costs are represented by affine functions.

It is important to emphasize that the technologies reviewed in this type of opti-

mization can be evaluated over very wide capacity ranges. Because of the linearity of the problem, determining correlations, particularly economic correlations, which enables to estimate an investment over a wide range with very low uncertainty, is a challenge. Thus, the economic results proposed in this study are intended to compare solutions. For this reason, it is assumed that that the scope of the various technologies are comparable and investment costs, operational costs are certain.

2.1.2 Thermal optimization

The optimization model involves thermal optimization via energy cascade calculation otherwise recoginised as *targeting*. This means that, at each time step, each heat flow is optimally utilized within the site to make the most of its heat and minimize the use of hot and cold utilities. However, it will not always be possible to achieve such a high level of thermal optimization on a real industrial site, due to the number of exchanges involved, the limited space available, load variations over time, or the distance between hot and cold sources. The cost of modifying the heat-exchanger network is not taken into account in this thesis, as it is highly dependent on the geometry and spatial configuration of the industrial site. If necessary, this assessment should be carried out during the conceptual study phase. Furthermore, as this modification to the network is not taken into account in any of the proposed optimizations, it is assumed that the network modification will not impact the order of solutions in terms of optimality.
It should be remembered that the purpose of this thesis is to provide a well-argued general decision-making aid. Thus, the key elements to be retained from the analysis are not the absolute values of the economic costs, but the relevance and robustness of the various solutions proposed.

It is important to clarify that this thesis does not focus on optimizing detailed process parameters like temperature, pressure, and recycle rate. Instead, the technologies are modeled from a generic perspective, and specific process parameters are not included in the optimization. These aspects could potentially be explored in a subsequent study, which would have a more focused technological scope.
The superstructure is the set of models representing the processes and different technologies studied and the inter-model links, coupled with the system constraints. The optimization of this superstructure is based on the resolution of the energy cascade and the use of linear technical-economic models.

Within the OSMOSE framework, after resolving the combined heat and mass model (targeting problem), the results provide optimal values for mass and thermal consumption by sizing the units appropriately. At this stage, all hot and cold thermal streams within the network can be enumerated, and several pinch points will be identified, which divide the temperature range into distinct subnetworks. Subsequently, Heat Load Distribution (HLD) will be applied to each subnetwork as an initial step before the detailed design of the heat exchanger network. HLD is formulated as a MILP model that aims to minimize the total number of connections among all hot and cold streams [Papoulias and Grossmann, 1983, François and Irsia,

1989, Floudas and Grossmann, 1986].

As an additional optimization layer, OSMOSE can solve for Heat Exchanger Network Synthesis (HENS), which is modeled as a Non-Linear Programming (NLP) problem [Floudas and Grossmann, 1987, Mian et al., 2016, Kermani, 2018, Kermani et al., 2019]. This optimization model aims to minimize the investment cost of the heat exchanger network among the set of hot and cold streams. The NLP problem formulation is based on the work of Floudas et al. [Floudas and Grossmann, 1987] for multi-time scenarios, though it is also applicable to single-time scenarios. The set of heat exchange connections is fixed by solving the HLD model, and the subsequent optimization focuses on optimizing the flows and temperatures within these fixed connections.

2.1.3 Mathematical formulation

The mathematical problem to be solved is defined as a MILP problem, which allows both discrete (binary) and continuous variables to be used.
The temporal dimension of the problem is taken into account with the intervals t belonging to T of duration d_{op}^{t} and allows to consider the variables and parameters of the problem as time-dependent. The system is represented by the set U of units u composed of a set PU of Process units and a set of Utility UU Utility units. Process units have a fixed capacity, representing for example some consumer demand. Utility units represent utility installations or connections to markets and networks, and are used to satisfy the needs of PU. These Utility units have a capacity between a minimum (f_u^{min}) and a maximum (f_u^{max}) bound. Each unit u can consume, supply or convert resources r, aggregate R, and heat, within the temperature ranges k. Mathematically, the dimensioning constraints are expressed as follows:

$$f_u^{min} = f_u^{max} = 1 \quad \forall u \in PU \tag{2.1}$$

$$y_{u,t} f_u^{min} \leq f_{u,t} \leq y_{u,t} f_u^{max} \quad \forall u \in U, \forall t \in T \tag{2.2}$$

$$y_{u,t} \leq y_u \quad \forall u \in U, \forall t \in T \tag{2.3}$$

$$f_{u,t} \leq f_u \quad \forall u \in U, \quad \forall\, t \ \in T \tag{2.4}$$

The variables $y_{u,t}$ and y_u are binary and reflect the selection of a utility, variables $f_{u,t}$ and f_u are continuous and represent used, or instantaneous, capacity and installed capacity respectively.
Each unit emits and/or consumes resources, $\dot{m}_{r,u,t}^{+}$ and $\dot{m}_{r,u,t}^{-}$ are the reference flow rates of a resource r produced or consumed, respectively, by the unit u at time t. More specifically, note the system's imports and exports $\dot{M}_{r,t}^{+}$ and $\dot{M}_{r,t}^{-}$ respectively. The equilibrium balance for each resource is given by the following equation:

$$\sum_{i=1}^{n_u} f_{ui}^{+} m_{ui,t}^{+} + M_{r,t}^{+} - \sum_{i=1}^{n_u} f_{ui}^{-} m_{ui,t}^{-} - M_{r,t}^{-} = 0 \quad \forall r \in R, \forall t \in T \tag{2.5}$$

Finally, the thermal cascade leads to the following equations, established for each thermal cluster where the units exchange flows $\dot{q}_{u,t,k}$. The heat balance is calculated

at each time step, over each k temperature interval. The residual heat $\dot{Q}_{t,k}$ of the cascade interval from high (k) temperatures to the lowest ($k-1$).

$$\sum_{u=1}^{n_{u,clu}} f_{u,t}\dot{q}_{u,t,k} + \dot{Q}_{t,k+1} - \dot{Q}_{t,k-1} = 0 \quad \forall t \in T, \quad \forall\ k \in K \tag{2.6}$$

$$\dot{Q}_{t,k} \geq 0 \tag{2.7}$$

$$\dot{Q}_{t,1} = \dot{Q}_{t,n_k+1} = 0 \quad \forall t \in T \tag{2.8}$$

The objective in this study is the minimization of Total Expenditure (TOTEX) defined according to Equation 2.9, composed of annualized investment costs $C_{Inv,an}$ and annual revenues R, the algebraic sum of revenues R_{val} and annual OPEX costs C_{op}.

Since the mathematical problem to be solved is linear, the operating and investment costs are also modeled as linear functions. These costs are expressed with a fixed component, $c_u^{op,fix}$ and $c_u^{inv,fix}$, and a variable part, $c_u^{op,var}$ and $c_u^{inv,var}$, associated with instantaneous and installed capacity, respectively. Instead of using potentially nonlinear cost functions, the decision was made to linearize and estimate these cost functions within their respective bounds, f_{min} and f_{max}, as a preprocessing task for the decision-maker. This approach avoids the need for piece-wise approximation methods for integrating nonlinear cost functions.
Nonlinear cost functions are common in industrial energy systems for various technologies, such as in the costs associated with the operation and maintenance of wind power plants and the scaling effects in the production of hydrogen via electrolysis [Kumbaroğlu and Madlener, 2012]

Annual revenues R_{val} are defined in Eq. 2.9 with a positive variable contribution $c_{r,t}^{-}$ in the case of the sale of a product or service. Operating costs as defined here, Equation 2.12, reflect the cost of equipment maintenance, or the purchase of materials and/or energy at unit price. $c_{r,t}^{+}$.
In Equation 2.13, the factor $\frac{\tau\ (1+\tau)^y}{(1+\tau)^y-1}$ is used to annualize investment costs. τ represents the discount rate and y the amortization period of the investment, in years.

$$\min(TOTEX) = C_{\text{Inv,an}} + C_{\text{op}} - R - R_{\text{val}} \tag{2.9}$$

$$R = R_{\text{op}} - C_{\text{op}} \tag{2.10}$$

$$R_{val} = \sum_{t=1}^{t_t} d_{op}^{t} \times \sum_{r=1}^{n_r} c_{r,t}^{-} \ \times\ \dot{M}_{r,t}^{-} \tag{2.11}$$

$$C_{op} = \sum_{t=1}^{t_t} d_{op}^{t} \times \left(\sum_{r=1}^{n_r} c_{r,t}^{+} \times \dot{M}_{r,t}^{+} + \sum_{u=1}^{n_u} \left[c_u^{op,fix} \times y_{u,t} + c_u^{op,var} \times f_{u,t} \right] \right) \tag{2.12}$$

$$C_{Inv,an} = \frac{\tau(1+\tau)^y}{(1+\tau)^y - 1} \times \sum_{u=1}^{n_u} \left(c_u^{inv,fix} \times y_{u,t} + c_u^{inv,var} \times f_u \right) \tag{2.13}$$

The impact of CO_2, denoted as $Emissions_{CO2}$, is formulated analogously to operating costs and is detailed in Equation 2.14. Here, the parameter $imp_{r,t}$ specifies the impact associated with the consumption/selling of a resource.

$$Emissions_{CO_2} = \sum_{t=1}^{t_t} d_{op}^{t} \times \left(\sum_{u=1}^{n_u} imp_u^{var} \times f_{u,t}^{+} \sum_{r=1}^{n_r} \left[imp_{r,t}^{+} \times \dot{M}_{r,t}^{+} - imp_{r,t}^{-} \times \dot{M}_{r,t}^{-} \right] \right) \tag{2.14}$$

2.2 Robust Optimization framework

Problem data in most optimisation applications are often unclear due to many factors such as market swings, unpredictability, regulatory changes, and other considerations. The final answer may not be optimal or feasible for practical applications in the actual world if the data uncertainty is ignored. Consequently, resolving uncertainty issues in optimisation is essential and has garnered significant attention from the corporate and academic sectors [Diwekar, 2003], [Sun and Conejo, 2021], [Ning and You, 2019]. Robust optimisation is a noteworthy method for addressing optimisation problems with uncertain data [Detienne et al., 2024]. Robust optimisation strategies begin with a predefined set in the uncertainty space and try to find the optimal solution for each data uncertainty realisation in the set. The equivalent optimisation problem is also known as a Robust Counterpart (RC) optimisation problem.
Because it doesn't require known probability distributions for uncertain parameters, this method stands out among other optimisation under uncertainty approaches. This makes it especially useful in applications where avoiding infeasibility is crucial or where determining such distributions is difficult. RO provides significant advantages over other optimization methods, especially in handling uncertainties. Unlike min-max optimization, RO allows for more flexibility in solution quality, particularly under varied scenarios. It maintains lower computational complexity compared to multi-stage stochastic and parametric optimization methods, even as the number of uncertain factors increases [García and Peña, 2018].

2.2.1 Motivation for robust optimization

In order to handle optimization problems under uncertainty and perturbed optimization problems, several techniques have been proposed. The most common approaches are sensitivity analysis, stochastic programming and RO, therefore it is important to note the difference between these aforementioned approaches and their respective difference with RO frameworks.

2.2.2 Robust Optimization versus Sensitivity Analysis

In sensitivity analysis, the initial stages of model construction and optimization do not take into account data uncertainty, with the focus instead being on justifying the solution obtained thereafter. Sensitivity analysis primarily serves to measure the

robustness of a baseline solution without providing insights on how to enhance this robustness. Particularly in models characterized by numerous uncertain parameters, conducting a comprehensive sensitivity analysis is often not feasible.
The fundamental distinction between sensitivity analysis and RO lies in their objectives and methodologies. Sensitivity analysis explores how variations in the problem's parameters might alter the optimal solution derived under standard conditions. On the other hand, RO is concerned with determining the extent to which the optimal solution of the standard problem might breach the constraints when the problem parameters are altered [Moazeni, 2006].

2.2.3 Robust Optimization versus Stochastic Programming

Stochastic programming models operate under the assumption that the probability distributions of uncertain input parameters are either known or can be reliably estimated. The objective in stochastic programming is to identify a solution that remains feasible across the majority of potential data scenarios, aiming to optimize the expected value of a function defined by the decision variables and random factors. The most prevalent and thoroughly investigated model in this domain is the two-stage (stochastic) linear programming.
A notable variant in stochastic programming is the chance-constrained programming model. This model allows for flexibility in meeting the requirements of the problem, as it does not necessitate a solution that adheres to all possible outcomes of the random parameters. Instead, it demands that solutions remain feasible within a pre-determined probability threshold.
The applicability of stochastic programming is confined to situations where uncertainties are stochastic in nature and their distributions are presumed to be known. Nonetheless, in practical scenarios, the exact distributions of these random parameters are rarely known and must be inferred from historical data. Consequently, any solutions derived from these models should be considered approximate [Moazeni, 2006].
The fundamental difference between the two lies in the fact that stochastic programming integrates the uncertainty by utilizing the probability distributions of parameters to anticipate and plan for a range of future scenarios, thus aiming for a solution that is optimal on average. RO, however, prepares for the worst possible scenario by ensuring that the solution is viable under any circumstances that might arise within the predefined bounds of uncertainty [Ben-Tal et al., 2009].

2.2.4 Uncertainty Set Induced Robust Optimization

Finding the optimal solution among those that are "immune" to data uncertainty—that is, candidate solutions that hold up for all realisations of the data from the uncertainty set—is the aim of set-induced robust optimisation. It is expected that the uncertain data fluctuates within a specific uncertainty set. Consider a general mixed integer linear optimisation problem with uncertainty in the objective function coefficients, left-hand side (LHS), and right-hand side (RHS), as presented in [Li et al., 2012]:

$$\max_{x,y} \sum_m \tilde{c}_m x_m + \sum_k \tilde{d}_k y_k$$
$$\text{s.t.} \quad \sum_m \tilde{a}_{im} x_m + \sum_k \tilde{b}_{ik} y_k \leq \tilde{p}_i \quad \forall i \tag{2.15}$$

where $\tilde{a}_{im}$,$\tilde{b}_{ik}$,$\tilde{c}_m$,$\tilde{d}_k$, and $\tilde{p}_i$ denote the true value of the uncertain parameters. The variables x_m and y_k are continuous and integer, respectively.
To shift all uncertainty to the LHS of the restrictions, the MILP problem might be reformulated as follows:

$$\max_{x,y,z} z$$

$$z - \sum_m \tilde{c}_m x_m + \sum_k \tilde{d}_k y_k \leq 0 \tag{2.16}$$

$$\tilde{p}_i x_0 \sum_m \tilde{a}_{im} x_m + \sum_k \tilde{b}_{ik} y_k \leq 0 \quad \forall i \tag{2.17}$$

Where $x_0 = -1$.
Li et al. [Li et al., 2012] concludes the analysis above by proposing a formulation of a (MI)LP problem that takes just LHS uncertainty into account and is based on a general i-th constraint, shown in Eq. 2.18.

$$\sum_j \tilde{a}_{ij} x_j \leq b_j \tag{2.18}$$

Where x_j can be an integer or continuous variable and $\tilde{a}_{ij}$ are subject to uncertainty. The uncertainty is defined as follows:

$$\tilde{a}_{ij} = a_{ij} + \xi_{ij} \widehat{a}_{ij} \quad \forall j \in J_i \tag{2.19}$$

Where a_{ij} represents the nominal value of the parameters, $\widehat{a}_{ij}$ represents positive constant perturbations, ξ_{ij} represents independent random variables which are subject to uncertainty and J_i represents the index subset that contains the variables whose coefficients are subject to uncertainty.
Now, the constraint Eq. 2.18 can be rewritten as Eq. 2.20 by regrouping the deterministic part and the uncertain part to the LHS.

$$\sum_j a_{ij} x_j + \sum_{j \in J_i} \xi_{ij} \widehat{a}_{ij} x_j \leq b_i \tag{2.20}$$

In set induced RO, the aim is to find the solutions that remain feasible for any ξ in the given uncertainty set U so as to immunize against infeasibility, thus constraint 2.20 becomes:

$$\sum_j a_{ij} x_j + \max_{\xi \in U} [\sum_{j \in J_i} \xi_{ij} \widehat{a}_{ij} x_j] \leq b_i \tag{2.21}$$

A wide variety of uncertainty sets have been described in the literature [Bertsimas et al., 2015]. Constraints with uncertain parameters must be feasible for all values

of the uncertain parameters in the uncertainty set, and correspondingly the objective value is taken to be the worst case value over all realizations of the uncertain parameters. For this reason RO problems, in their original statement, typically have an infinite number of constraints and cannot be solved directly. The most common approach to date for solving them in the literature is to use duality theory [Vayanos et al., 2020] to reformulate them as a deterministic optimization problems (RC) that may have additional variables, constraints, and even change problem class (e.g., a robust LP problem with an ellipsoidal uncertainty set becomes a second-order cone problem [Ilyina, 2017]).
The formulation of the RC is connected to the selection of the uncertainty set U. There are, as stated before, several classical definitions of uncertainty sets for bounded uncertainties in RC optimization, including box, ellipsoidal and polyhedral uncertainty sets ([Zhang et al., 2016], [Li et al., 2012], [Ben-Tal et al., 2009]).
According to the uncertainty sets defined by the Euclidean norm, uncertain parameters can be considered within a multidimensional space, where the dimension is equal to the cardinality of uncertainty sets. The size of uncertainty set is decided by the selected norm and its adjustable parameter. For two uncertainties $\tilde{a}_1 = a_1 + \xi_1\widehat{a}_1$,$\tilde{a}_2 = a_2 + \xi_2\widehat{a}_2$, their norm-based uncertainty sets can be presented from the geometric view in two dimensional space, which are shown in Figure 2.2 [Zhang et al., 2016].

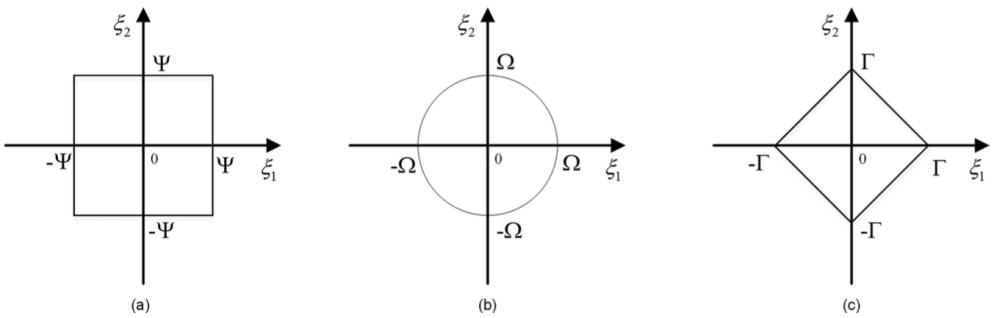

Figure 2.2: Geometric view of classical uncertainty sets: (a) box uncertainty set; (b) ellipsoidal uncertainty set; and (c) polyhedral uncertainty set, where Ω, Ψ, Γ are the adjustable parameters of the set formulations [Zhang et al., 2016].

For the RC, this thesis will focus on box uncertainty sets since a box uncertainty set reformulation doesn't change the problems linearity as supposed to for example ellipsoidal uncertainty sets who's RC becomes a second-order cone problem.
The mathematical form of an box uncertainty set is defined as follows [Li et al., 2012]:

$$U_\infty = \{\xi_j : |\xi_j| \leq \Psi, \forall j \in J_i\} \tag{2.22}$$

Which can be reformulated as a RC as:

$$\begin{cases} \sum_j a_{ij}x_j + \Psi \sum_{j\in J_i} \hat{a}_{ij}u_j \leq b_i, \\ -u_j \leq x_j \leq u_j \end{cases} \tag{2.23}$$

where Ψ is the adjustable parameter, and the suggested range is $\Psi \leq 1$; u_j is a positive intermediate variable.

2.2.4.1 Continuous Uncertainty with Confidence Level

It's relatively straightforward to compute the percentage of uncertain values that reside within a specified range, provided that the probability density functions of continuous uncertainties are available. Continuous uncertainties without bounds can be transformed into bounded uncertainties using a "confidence level". Consequently, any extreme uncertain values that exceed these bounds may be disregarded. In this context, bounds can be established using quantile values when the "confidence level" $1-\gamma_i$ for the i-th constraint is defined. Indeed, the confidence level can be independently determined for each uncertainty as $1-\gamma_{ij}$, though confidence levels are generally represented uniformly as $1-\gamma_i$. Therefore, the uncertainty $\tilde{a}_{ij}$ can be characterized as:

$$\tilde{a}_{ij} = a_{ij}^{1-\gamma_i} + \xi_{ij}\widehat{a}_{ij}^{1-\gamma_i} \tag{2.24}$$

Where:

$$a_{ij}^{1-\gamma_i} = \frac{F_{\widehat{a}_{ij}}^{-1}(\frac{\gamma_i}{2}) + F_{\widehat{a}_{ij}}^{-1}(\frac{1-\gamma_i}{2})}{2} \tag{2.25}$$

$$\widehat{a}_{ij}^{1-\gamma_i} = \frac{\left|F_{\widehat{a}_{ij}}^{-1}(\frac{1-\gamma_i}{2}) - F_{\widehat{a}_{ij}}^{-1}(\frac{\gamma_i}{2})\right|}{2} \tag{2.26}$$

Where F^{-1} is the inverse cumulative distribution function (quantile function) of the probability distribution of $\widehat{a}_{ij}$ and the uncertain range is decided by ξ_{ij}. A ratio parameter is defined $c_{ij} = \frac{\widehat{a}_{ij}^{1-\gamma_i}}{\widehat{a}_{ij}^{max}}$ for any $j \in J_i$ to represent the ratio of considered width and the exact width of the uncertain interval. $\widehat{a}_{ij}^{max}$ represents the maximum range of uncertainty.
Thus, the newly defined adjustable parameter can be used for determining the changeable range of every individual uncertainty as:

$$\widehat{a}_{ij} = a_{ij}^{1-\gamma_i} + \xi_{ij}a_{ij}^{max}, \quad \xi_{ij} \in [-c_{ij}, c_{ij}] \tag{2.27}$$

2.2.4.2 Flexible Uncertainty set

The vector of the uncertain variable ξ_{ij} can be used to focus attention on all of the continuous uncertainties in the optimisation model, based on the concept of bounded uncertainty in Eq. 2.24. Consequently, the Euclidean norms of vectors associated with ξ continue to provide the basis for the definition of the flexible uncertainty sets. The estimated outcomes of uncertainties and the selected confidence level are related to the given boundaries. Every ratio parameter of uncertainty in the uncertainty set can have an impact on the traditional adjustable parameter when incorporating c_{ij} to the classical uncertainty sets.

$$U'_{\infty} = \left\{\xi \mid \|\xi\|_{\infty} \leq \Psi, \Psi = \max_j c_{ij}, \forall j \in J_i\right\} \tag{2.28}$$

Where the adjustable parameter Ψ is decided by the maximum of ratio parameter c_{ij}, which means the size of the uncertainty set is controlled by independent confidence levels of uncertainty.
Then the corresponding RC constraint Eq. 2.21 is equivalent to:

$$\begin{cases} \sum_j a_{ij}^{1-\gamma_i} x_j + \Psi \sum_{j \in J_i} \hat{a}_{ij}^{max} u_j \leq b_i, \\ -u_j \leq x_j \leq u_j, \quad \forall j \in J_i, \\ \Psi = \max_j \{c_{ij}\}, \quad \forall j \in J_i. \end{cases} \tag{2.29}$$

A detailed reformulation of Eq. 2.12 can be found in Appendix A.

2.2.4.3 Probility bounds of uncertainty sets

A fundamental aspect of RO is the necessity for an explicitly defined uncertainty set before attempting to solve the problem. However, in practical scenarios, decision-makers often provide only approximate bounds for these sets. The expectation for decision-makers to define an uncertainty set with precision is frequently unrealistic, particularly given the pervasive nature of uncertainty across numerous domains. This approximation can lead to significant challenges in RO, notably when strict adherence to all constraints potentially renders a problem infeasible or drives the objective value far from the optimal value of the nominal problem [Karimi, 2012].
Addressing the challenge of accurately defining uncertainty sets, it is useful to consider probabilistic bounds. As proposed by Li et al. and Bertsimas et al. ([Li et al., 2012], [Bertsimas et al., 2021]), probabilistic bounds offer a systematic approach to quantify the reliability of an uncertainty set in terms of constraint satisfaction. Two key questions arise in this context: Firstly, what is the necessary size of the uncertainty set to ensure that the degree of constraint violation remains within acceptable limits? Secondly, once a RO problem is solved, what is the actual degree of constraint violation observed?

The methodology to answer these questions involves two different approaches. The first is determining what is known as the *a priori* probability bound, which is derived directly from the RC constraint formulated from the uncertainty set itself. This bound provides an initial probabilistic guarantee on the likelihood of satisfying the constraints before the actual optimization occurs. The second approach assesses the *a posteriori* bound, which is calculated from the solution of the RO model. This method effectively evaluates the actual probability of constraint violation post-optimization.
Both approaches allow for the derivation of different probability bounds based on varying levels of uncertainty information. These probabilistic bounds are crucial for providing decision-makers with a quantifiable measure of risk associated with potential constraint violations, thereby enhancing the practical applicability and reliability of RO models.
Since a probabilistic bounds approach is outside the scope of this thesis, the methodology suggested by Zhang et al. [Zhang et al., 2016] will be employed for the purpose

of simplicity and accessibility. According to Section 2.2.4.1, the adjustable parameters in this method are defined as ratios. See Zhang et al. for further information on the probabilistic boundaries on these formulations.

2.3 Hot gas approach

In the modelling framework, boilers and furnaces are modeled using the "hot gas approach" [Maréchal and Kalitventzeff, 1998]. The advantage of this method is that heat is available for any use. Coupled with the steam-energy equivalence developed for steam uses and supply detailed in Section 2.4.
The hot gas approach consists in considering that the combustion of gas in air produces two heat flows, a first radiative flow at very high temperature, and a second, convective flow at lower temperature. T_{ad}^{corr} is the adiabatic combustion temperature of the gas in air for the gas burned corrected for excess air, Eq. 2.30. The heat flows are characterized by the following equations. The radiative flux Q_{Rad}, Eq. 2.31, is available at T_{rad} with a pinch of 2°C, and the convective flux Q_{Conv}, Eq. 2.32 is available between T_{rad} and T_{Chem} with a pinch of 15°C.

$$T_{ad}^{corr} = T_0 + \frac{1}{\frac{1}{T_{ad}-T_0} + c_p^{air} \times (n-1) \times \frac{m_{st}^{air}}{3600 LHV}} \tag{2.30}$$

$$Q_{Rad} = \frac{T_{ad}^{corr} - T_{rad}}{T_{ad}^{corr} - T_0} \times \dot{n}_{gaz} \times LHV \tag{2.31}$$

$$Q_{Conv} = \frac{T_{rad} - T_{Chem}}{T_{ad}^{corr} - T_0} \times \dot{n}_{gaz} \times LHV \tag{2.32}$$

with:

- T_{ad}^{corr} is the adiabatic combustion temperature of the gas in air, corrected for excess air;
- T_{ad} the adiabatic combustion temperature of the gas in stoichiometric air, at 1952°C;
- n the air factor, here 1.05;
- c_p^{air} the average heat capacity of air between T_{rad} and T_0 is 1.08 $kJ \cdot K^{-1} \cdot kg^{-1}$;
- NCV the lower heating value of the gas mixture fed to the boiler, in $\frac{kWh}{Nm^3}$;
- m_{st}^{air} the stoichiometric air mass is $1.104 \frac{kg}{kWh_{LHV}}$;
- T_{rad} the emission temperature of the radiative flux;
- $\dot{n}_{gaz}$, gas flow to the in $\frac{Nm^3}{h}$;
- T_{Chem} the atmospheric emission temperature of the fumes, 150°C;
- T_0 reference temperature of 25°C.

2.4 Steam energy

Firstly, the thermal problem is decoupled from the mass problem. In fact, by consuming steam, customers (internal or external) express a need for heat, which is

satisfied by consuming steam and (partially) returning condensates. The most relevant approach for linking mass aspects (feedwater consumption, hot condensate return) and energy aspects (consumption of desuperheating, condensation and subcooling heat) is as follows. For a demand $\dot{m}$ ($\frac{kg}{h}$) for steam at pressure P_{Client} (bara) and temperature T_{Client} (°C), with condensate return rate R_{Client}, the thermal model follows Equations 2.33-2.35, where T_{Stat} is the saturation temperature of steam at pressure P_{Client}, and h is the enthalpy of mass of water for the different states specified in subscript: in the superheated state for h_{gas}, in saturated steam and liquid for $h_{Sat,g}$ and $h_{Sat,l}$ respectively, and in the liquid state of condensate return for h_{cond}. The saturation temperature and enthalpy values are obtained dynamically via the CoolProp database [Bell et al., 2014].
With these 3 equations, the heat flow Q (W) is discretized according to the 3 contributions of desuperheating, latent heat of condensation and subcooling, in accordance with the temperature range involved.

$$Q_{gaz} = \frac{\dot{m}}{3600}(h_{gas} - h_{Sat,g}) \quad \text{for} \quad [T_{Client}\ ;\ T_{Stat}] \tag{2.33}$$

$$Q_{latent} = \frac{\dot{m}}{3600}(h_{Sat,g} - h_{Sat,l}) \quad \text{at} \quad T_{Stat} \tag{2.34}$$

$$Q_{liq} = \frac{\dot{m}}{3600}(h_{Sat,l} - h_{cond}) \quad \text{for} \quad [T_{Stat}\ ;\ T_{cond}] \tag{2.35}$$

The mass balance is expressed by the following equation:

$$\dot{m}_{cond} = \dot{m} \cdot R_{Client} \tag{2.36}$$

3
Methods

This chapter outlines the development of the energy technologies incorporated into the optimization model. Initially, the base case models are introduced in Section 3.1. Subsequently, the technologies implemented for decarbonization are detailed in Section 3.2. Following this, Section 4.1 presents a comprehensive industrial cluster as an illustrative example for the optimization model. In Section 4.1.1, the established energy consumption parameters for various consumers are provided to feed to the optimization model. Finally, Section 4.2 investigates and processes the uncertainties to be integrated into the robust model for electricity and gas prices.
Since the natural gas-fired boilers and conventional biomass boilers are essentially modeled as conventional furnaces/boilers, their thermal integration figures are redundant. The most crucial aspect is the approach specified in Section 2.3 for these technologies.

3.1 Base case models

The base case models represent the existing technologies and are thus exempt from investment cost considerations. This baseline is established as a reference point featuring conventional technologies, including gas-fired boilers, CHP units, a water plant to recover condensate and provide preheated water to boilers, and cooling utilities such as the cooling tower and absorption chiller. These components will be elaborated and detailed further in this section.

3.1.1 Natural gas Boilers

Each boiler has a nominal capacity of 90 t/h, with a minimum production rate of 40%. The steam produced is at high pressure (86 bar) and is superheated to 205°C. The boilers are fueled with natural gas, whose composition is taken from [Faramawy et al., 2016]. It is assumed that there is 5% excess air above the stoichiometric requirement. For production of 90 t/h of steam requires the combustion of 90542 kW_{HHV} of natural gas considering an overall efficiency of 94% [Vakkilainen, 2017].

3.1.2 Cooling tower

Chilled water is produced by mechanical draft cooling tower. The water temperature at the start of the tower is 27°C, and the return temperature is 37°C. The associated power consumption is ≈ 0.02 kWe per kW [Turton et al., 2018] of cooling output.

3.1.3 Steam superstructure

To ensure effective steam distribution, a network with varying pressure levels is developed according to the needs of the consumers. Each consumer returns a fraction of its steam demand (Return Rate) as hot liquid condensate. These condensates are recycled as much as possible through cooling, purification, and preheating processes before being fed back into the boilers and CHP units. Any fraction that cannot be reused due to excessively low temperature is discharged, and make-up water is supplied as needed.

3.1.4 Cogeneration engine utilities

Two different cogereration units are considered: a larger 18MW system that integrates four engines, using specifications from [Jenbacher, 2023b], and a smaller, 2.6MW unit, detailed according to [Jenbacher, 2023a]. These CHP units have the capability to produce saturated steam at 8bara with a Heat Recovery Steam Generator (HRSG), valorizing the thermal energy from flue gases cooled from 450°C to 160°C. For a breakdown of the energy inputs and outputs associated with these CHP configurations, refer to Table 3.1. Information regarding the properties of the flue gases used for these calculations is taken from [Salazar et al., 2013].
The integration into the modelling superstructure can be seen in Figure 3.1.

	CHP 1 (4x)	**CHP 2**
Engine		
$P_{\text{elec, Nom}}$ (MWe)	4.404	2.679
η_{e} (kWe/kW_{LHV})	0.467	0.457
$Q_{\text{gas, Nom}}$ (MW_{HHV})	10.35	6.43
$Q_{\text{fluegas, Nom}}$ (MW)	1.42	0.88
Boiler		
Q_{Nom} (kW)	1421	883
$m_{\text{steam, Nom}}$ (t/h)	2.14	1.33

Table 3.1: Energy parameters CHP 1 and 2.

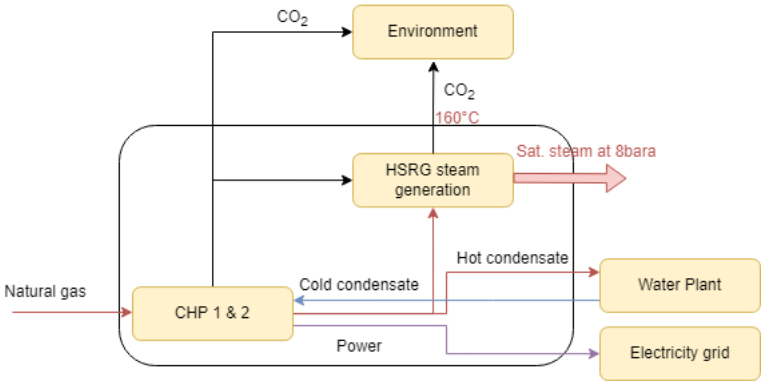

Figure 3.1: Cogeneration engine model, and steam generation is optional.

This utility is bounded by $f = \{0, 1\}$

3.1.5 Absorption chiller

The absorption chiller is a thermodynamic machine that uses heat in this case at 95°C with additional electricity to produce cold (7-12°C) and medium-temperature water (approx. 30-40°C). The technical details are taken from Hoffschmidt et al. ([Hoffschmidt et al., 2022]) and Energie Plus Le Site (2024) ([Energie Plus Le Site, 2024]) and are as follows:

1. In the evaporator, the refrigerant (in this case water) is sprayed into a low-pressure environment. A water circuit runs through the evaporator. As the refrigerant evaporates, it removes heat from the water, which is then cooled. Some of the sprayed refrigerant does not evaporate, but falls to the bottom of the evaporator, where it is pumped out and sprayed again.
2. The water vapour created in the evaporator is fed to the absorber. The absorber contains the absorbent solution, which is continuously pumped to the bottom of the container for spraying. The absorbent solution absorbs the water vapour out of the evaporator, thus maintaining the low pressure required to vaporize the refrigerant.
3. As it absorbs water vapour, the absorbent solution becomes increasingly diluted. Eventually, it becomes saturated and can no longer absorb anything.
4. The solution is then regenerated in the generator. It is heated by a hot-water stream (approx. 95°C) and some of the water evaporates. The regenerated solution returns to the absorber.
5. Finally, the steam extracted from the generator is fed to the condenser, where it is cooled by cold water circulation. The condensed water returns to the evaporator.

The data on the performance of the units utilized in this research were sourced from [LG, 2023]. It includes a Coefficient of Performance (COP) of 0.74 for a temperature difference (ΔT) of 95°C to 55°C for the hot water stream, and a COP of 0.72 for a ΔT of 95°C to 80°C.

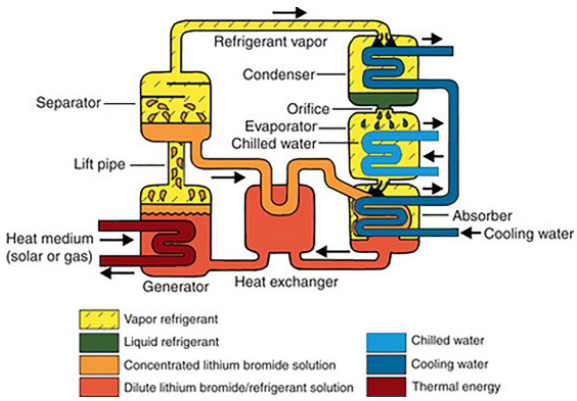

Figure 3.2: Absorption chiller operation [Hoffschmidt et al., 2022].

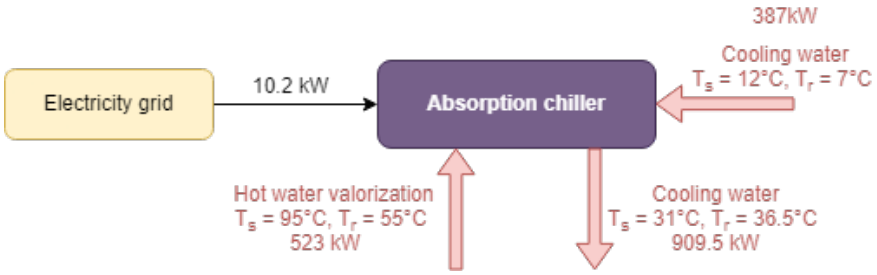

Figure 3.3: Absorption chiller model. This unit consumes electricity and heat at 95°C to produce chilled water (7-12°C). In return, medium-temperature heat is emitted. Red arrows indicate connections to the thermal cascade. Data from [LG, 2023]

.

The economic details for utilizing an absorption chiller, including both the initial investment and ongoing operational expenses, are derived from [U.S. Department of Energy, 2017]. This source provides a comprehensive examination and comparison of absorption chillers of various capacities. Specifically, the upfront investment required for the absorption chiller is noted as 5500EUR per ton of chilled water capacity, accompanied by an operational cost of 0.6¢per ton of chilled water.
The absorption chiller models are not bounded in capacity.

3.2 Decarbonisation models

3.2.1 Biomass fired boiler

The biomass fired boiler is designed following the same principles as the hot gas approach detailed in section 2.3. This boiler combusts up to 9 tons per hour of wet biomass. The biomass data used is sourced from [Sweeten et al., 1986]. Information regarding the biomass is summarized in Table 3.2. Co_2eq is calculated according to the composition stated in [Sweeten et al., 1986].

	Wet	**Dry**
Fresh cattle manure		
LHV $(\frac{kWh}{kg})$	3.78	4.49
HHV $(\frac{kWh}{kg})$	4.15	4.82
CO_2eq $(\frac{kgeq.CO_2}{kg})$	1.43	1.66

Table 3.2: Combustion data biomass **from** [Sweeten et al., 1986].

The biomass fired boiler is bounded in capacity of $f = \{0.5, 1\}$.

3.2.2 Amine capture

Amine capture is a commonly studied solution for capturing CO_2 in flue gases [Panja et al., 2022]. This solution involves the chemical absorption of CO_2 in an aqueous

amine solution. A typical scheme is shown in Figure 3.4. CO_2-rich flue gas enters at the bottom of the absorption column and exits at the top with a reduced CO_2 content. The concentrated CO_2 stream (90% of the incoming CO_2) exits at the condenser associated with the stripper. Data from [Danish Energy Agency, 2023] was used to build this model.

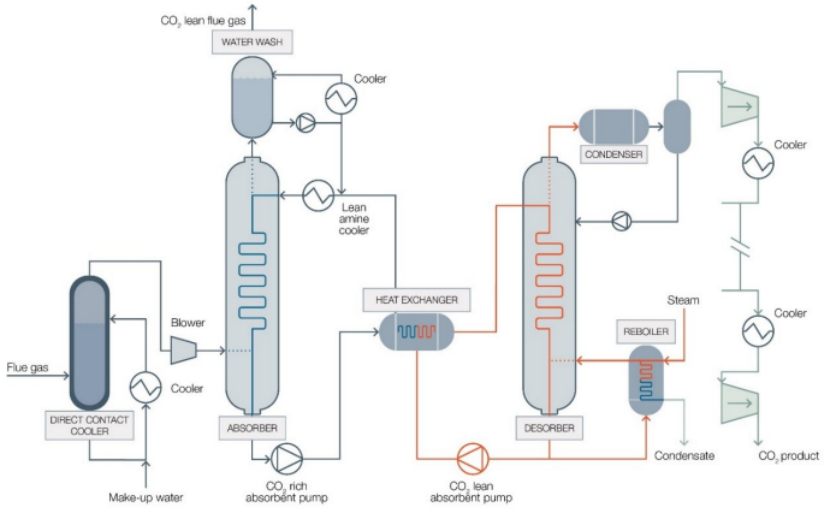

Figure 3.4: Schematic diagram of a typical CO_2 capture system with amines [Danish Energy Agency, 2023].

The following model is implemented in the model superstructure:

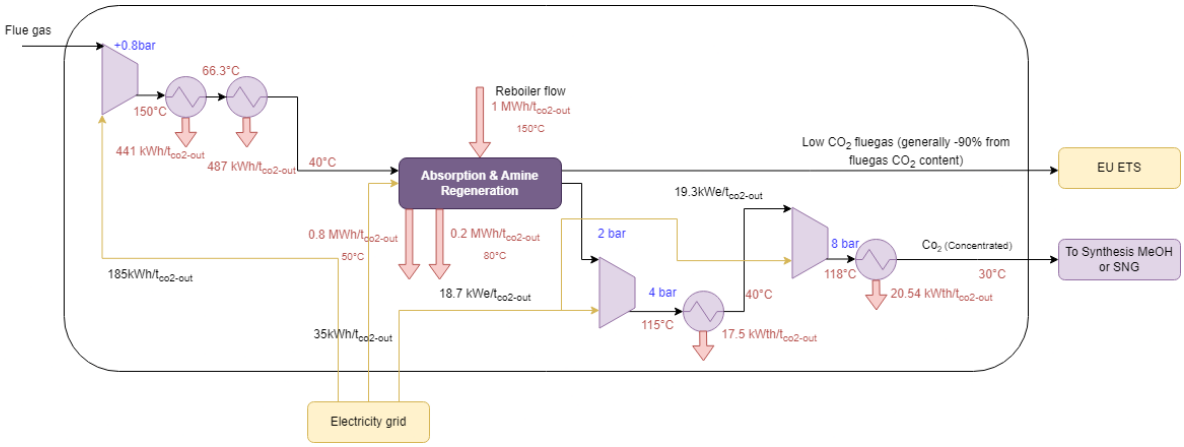

Figure 3.5: CO_2 capture unit model of amine contact combustion units. The model contains the P,T adaptation of the incoming and outgoing streams. Data from [Danish Energy Agency, 2023]

.

As the literature data are valid for an incoming flow at 40°C, there might be additional cooling needed at plant level to provide to the capture plant, The approach temperature for the gas-only exchanger is 10°C, and is set at 2°C for the partial condensation section. The electrical and thermal power requirements are shown in

the diagram in Figure 3.5. The concentrated CO_2 is emitted at the stripper outlet at 2 bara. To ensure consistency with possible uses in the superstructure, a double compression stage with intermediate cooling is added to reach 8 bara. This compression can be provided either by reciprocating compressors (stage output between 135 and 3000 kW) or by positive displacement compressors for stage outputs between 18 and 135 kW.

The economic data for the amine capture plant is based on [Danish Energy Agency, 2023] reporting on the projection of costs of amine capture plants (see Figure 3.6)

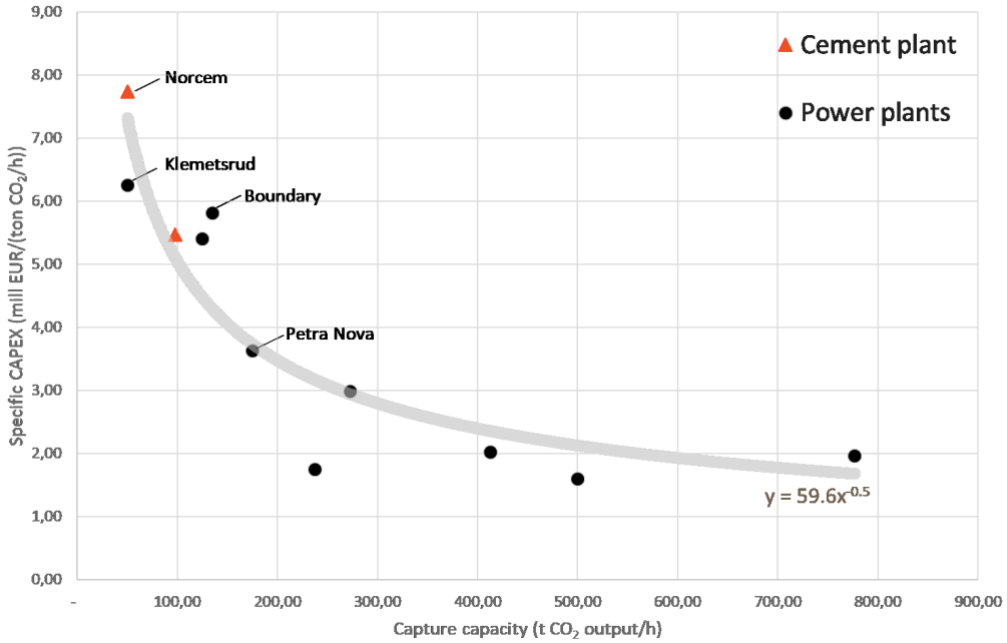

Figure 3.6: Specific CAPEX cost of complete CC plant installation including CO_2 liquefaction, integration and utility costs vs. CC plant capacity [Danish Energy Agency, 2023].

Since the size of the reference amine CC model is quite small compared to the reported CC installations, a reference CAPEX is chosen of 6M EUR/tCO_2 captured. In addition to electricity and heat consumption, annual OPEX are considered at 3% of CAPEX for the fixed contribution and 2.5 $\frac{EUR}{h}$ per tCO_2 captured for amine consumption. The amine CO_2 capture plant's capacity is bounded by $f = \{0.3, 5\}$.

For flue gas pre-treatment, the costs tabulated in the Chauvel method [Chauvel et al., 2001] are used for the booster, and the two exchangers are also costed using the correlations proposed by [Turton et al., 2018] set at adding 3.05MEUR to the investment cost. The various installation and other factors used to obtain the total module cost are taken into account.

For CO_2 outlet compressors,Turton's tabulated data rotary or reciprocating compressors is used [Turton et al., 2018]. In addition to electricity consumption, an annual OPEX worth 5% of the installed cost is considered.

3.2.3 Oxyfuel combustion

In traditional combustion methods, air is utilized as the oxidizing agent, which introduces nitrogen (N_2) into the mix, thereby diluting the concentration of CO_2 in the flue gas. This dilution complicates and increases the cost of CO_2 capture due to its reduced concentration. In contrast, oxy-fuel combustion employs either pure oxygen (O_2) or a combination of CO_2 and O_2 as the combustion reactants, eliminating the presence of nitrogen. Consequently, the flue gas generated is predominantly composed of CO_2 and water vapor (H_2O). To obtain nearly pure CO_2, the water vapor is separated from the flue gas through a condensation process, facilitating the capture of CO_2 in a concentrated form [Saha and Dally, 2022].
The oxy-fuel combustion process involves mixing the oxygen stream with recycled flue gas (RFG) to create an oxygen-rich gas mixture for combustion, as illustrated in Figure 1. This recycling of flue gas is crucial for controlling the potentially excessive flame temperatures that pure oxygen combustion would generate [Zheng et al., 2015].

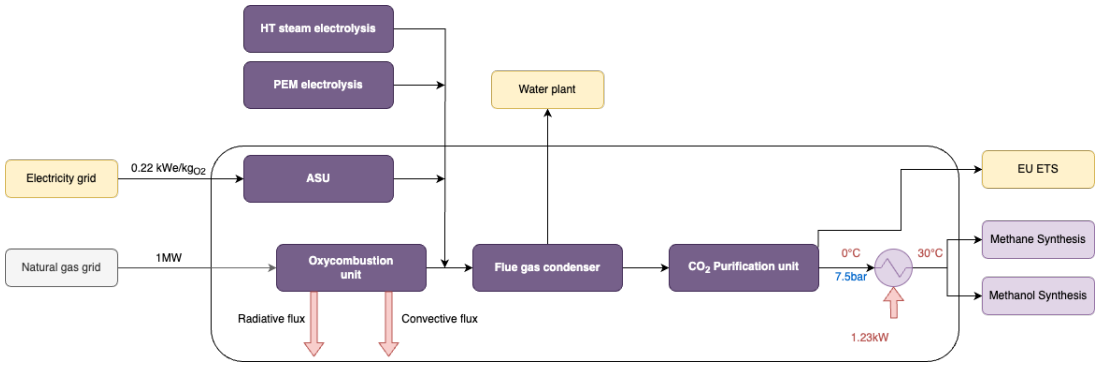

Figure 3.7: Model of the oxy-fuel combustion unit, comprising the ASU for oxygen production, the oxy-fuel boiler, the flue gas condenser and the CO_2 purification unit (CPU)

The model is based on a generic natural gas fired Oxyfuel furnace. The electrical consumption of the ASU is taken from [Danish Energy Agency, 2023].
The Oxycombustion model is bounded by $f = \{0, 200\}$.

3.2.4 Electrolysis PEM

PEM electrolysis transforms demineralized water in its liquid state into hydrogen (H_2) and oxygen (O_2), as outlined in the reaction in 3.1. This process demands a significant amount of electrical energy primarily to split the water molecule and to offset the electrical fluctuations resulting from the different electrical and electrochemical occurrences associated with this type of reaction [de Saint Jean, 2014].

$$H_2O_{liq} \leftrightarrow H_2 + \frac{1}{2}O_2 \tag{3.1}$$

The demineralized water supplied to the unit is introduced at room temperature, while the electrolysis reaction occurs within a temperature range of $50 - 100°C$.

The specific energy consumption for PEM electrolysis is approximately 4.8 kWh per cubic meter of hydrogen (Nm^3H_2), which equates to 53.3 kWh per kilogram of hydrogen ($\frac{kWh}{kgH_2}$). This estimation is derived from the specifications detailed in [Enapter AG, 2023].

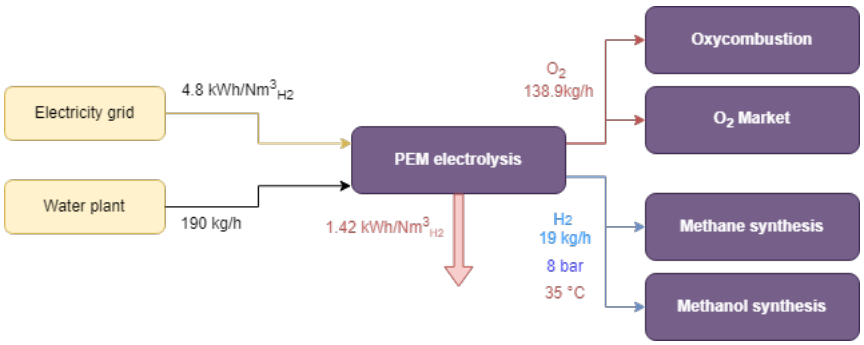

Figure 3.8: Model of water electrolysis unit for hydrogen production, Proton Exchange Membrane (PEM) technology. Data from [Enapter AG, 2023]

Financial estimates for large-scale hydrogen units via PEM electrolysis have been deduced from information provided by [International Renewable Energy Agency (IRENA), 2020], which highlights a total system expense ranging from 700 EUR to 1400 EUR per kW for installations exceeding 10 MW capacity. The benchmark cost is set at 980 EUR per kW for a system size of 5 MWe. Consequently, for a system capacity of 20 MWe, the estimated cost stands at 625 EUR per kWe, aligning with projections made for the period from 2020 to 2030 as suggested by [Zauner et al., 2019]. The PEM electolyser is bounded by $f = \{0.2, 60\}$
Moreover, the annualized value of the investment, as calculated within the modelling framework, encompasses the cost associated with replacing the stacks. It's assumed that these stacks require replacement every 8 years. The expenditure for each replacement is projected to be 20% of the initial investment cost. When this replacement expense is discounted and averaged out over a 20-year operational period, it results in an increase of 13.7% in the annualized cost of the equipment. Since the primary data reflects the total system cost, no additional expenses are considered. OPEX, which do not include the cost of water and electricity, are calculated to be 2.5% per year of the CAPEX, excluding the costs related to replacement.

3.2.5 High-temperature Electrolysis (SOEC)

High-temperature electrolysis utilizes solid oxide electrochemical cell (SOEC) technology, which offers the benefit of directly converting water supplied in vapor form, resulting in enhanced efficiency. Specifically, the energy consumption is approximately $3.6kWh$ per cubic meter of hydrogen ($\frac{kWh}{Nm^3H_2}$), as cited in [Sunfire GmbH, 2023]. This is more energy-efficient compared to low-temperature electrolysis methods such as or PEM or alkaline electrolysis, because it requires a lower input of electrical energy. This efficiency gain is due to a portion of the energy requirement being met through thermal energy, which is introduced upstream during the vaporization of water.

$$H_2O_{vap} \leftrightarrow H_2 + \frac{1}{2}O_2 \tag{3.2}$$

For the high-temperature electrolysis unit outlined in this model, data is obtained from [Sunfire GmbH, 2023]. The pressure of the steam feed is selected to be at the lowest possible level within the specified range (4.5-5.5 bara) to ensure that the temperature required for water vaporization is minimized. In this scenario, hydrogen is generated at a pressure of 1 bara. Therefore, a three-stage compression process with intermediate cooling stages is implemented to increase the pressure to 8 bara.

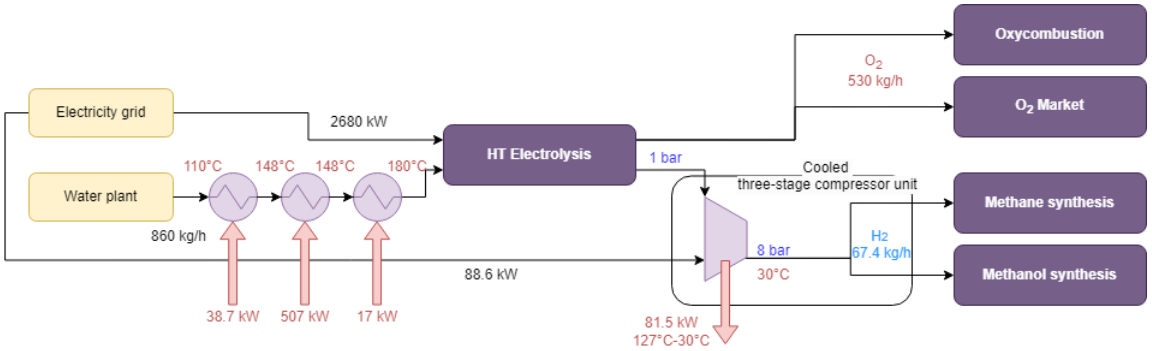

Figure 3.9: Model of water vapor electrolysis unit for hydrogen production, SOEC technology. Data from [Sunfire GmbH, 2023].

The investment cost calculations are based on the total cost of the complete system, which amounted to 1990 EUR per kWe for a capacity of $5MWe$ in 2020. For a system with a capacity of $100MWe$, the estimated cost is 875 EUR per kWe, a figure that aligns with projections made for the period between 2020 and 2030 according to [Zauner et al., 2019]. The SOEC electrolyser capacity is bounded by $f = \{0, 600\}$.

3.2.6 Catalytic Methanol Synthesis

The data for methanol synthesis used in this superstructure are derived from [Fernández-Dacosta et al., 2019]. The process diagram modeled is illustrated in Figure 3.10. For effective performance regarding reactant conversion, methanol selectivity, and minimizing the risk of carbon deposit formation on the catalyst, the reaction should be conducted at a high pressure (50-80 bar). Additionally, it is crucial to manage the temperature increase resulting from the reaction's exothermic nature, as indicated in the reaction 3.3.

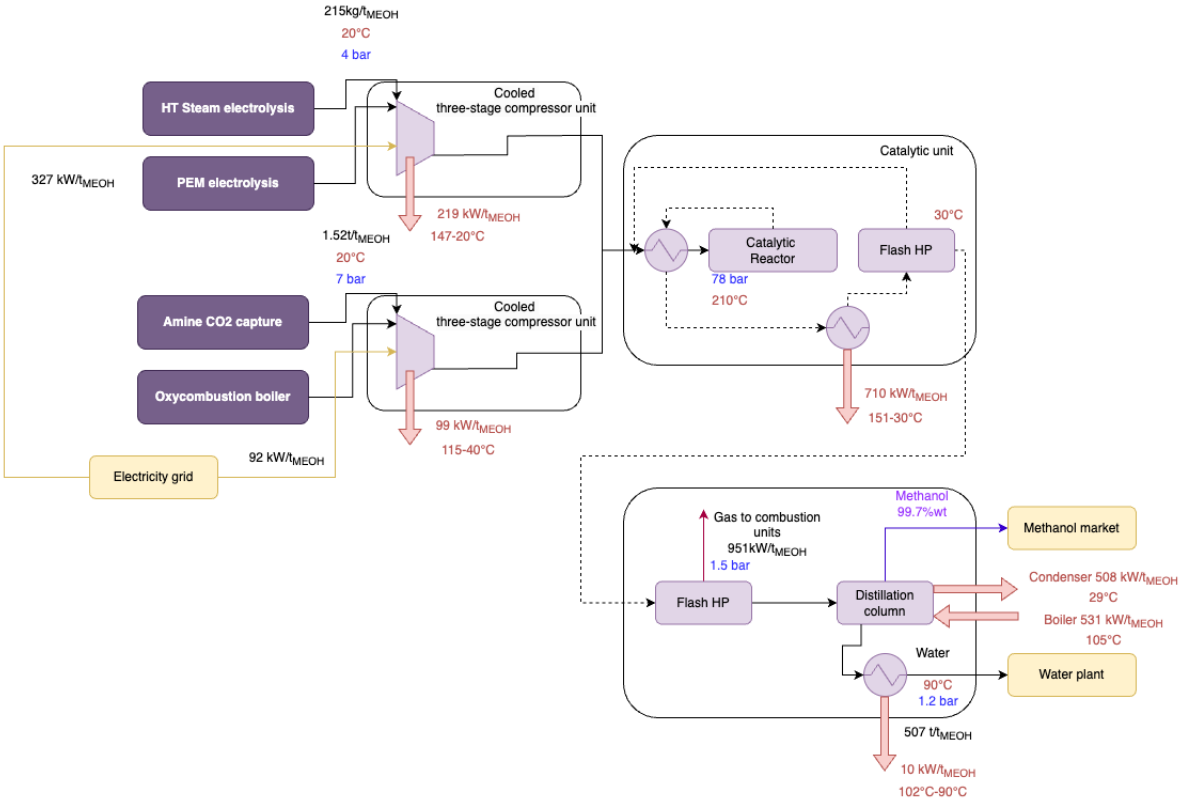

Figure 3.10: Model of the catalytic methanol synthesis unit, consisting of the reagent compression section with a triple stage with compressor with intercooling, followed by catalytic synthesis and finally methanol concentration by distillation. Data from [Fernández-Dacosta et al., 2019].

$$CO_2 + 3H_2 \leftrightarrow CH_3OH + H_2O; \quad \Delta H^0 = -49.5kJ/mol \tag{3.3}$$

In alignment with the inlet conditions described by [Fernández-Dacosta et al., 2019] for the process, the reactants are initially compressed to 79 bara using cooled multi-stage compressor units and subsequently preheated to 210°C prior to being introduced into the adiabatic catalytic reactor. The resulting hot gases are then cooled and flashed at 30°C. The gaseous portion is recycled back to the beginning of the process, while the liquid phase, predominantly consisting of water and methanol, undergoes flashing at low pressure. This separates out a gaseous fraction that can be utilized through combustion, and the remaining liquid is directed into a distillation column to isolate methanol from water. The produced methanol is 99.7%wt pure and is ready for export. Lastly, the water exiting the column is 90% recycled, after being cooled to $90°C$.
The economic analysis is based on data from [Nyári, 2018], which examines methanol production capacities of $50\frac{kt}{year}$ and $250\frac{kt}{year}$. The data on the purchase prices of equipment cover the reactor, distillation column, flash separators, and half of the compressors. Since the only compressor that overlaps within this system is the recycle compressor, the compressors for the H_2 and CO_2 inlet compression are considered separately. The fixed investment cost is considered at 9.45MEUR and an

additional variable investment cost of 9MEUR for a methanol plant producing 12.6 t/h of $MeOH$.
OPEX are estimated at $4\frac{\%}{year}$ of the installed costs.
H_2 and CO_2 are supplied to the methanol synthesis unit at 7 bara from other units. The technical and economic models include compressing these gases to 78 bara in three stages, with intermediate cooling after each stage.
For estimating installation costs, the correlations provided by [Turton et al., 2018] are applied, considering rotary compressors for smaller capacities ($18 - 135$ kW per stage) and reciprocating compressors for higher capacities ($135 - 3000$ kW per stage). The overall module cost is factored into the calculations. Operating costs are presumed to be $5\frac{\%}{year}$ of the module's total cost. The methanol's capacity is bounded by $f = \{0, 5\}$.

3.2.7 Electric Boiler

Investigating electric boilers offers a promising alternative for providing process heat in the shift towards electrification, especially as replacements for heat generation systems powered by fossil fuels. Electric boilers produce saturated steam, requiring the addition of a superheater to achieve the desired steam quality. These systems are very flexible, with the capability to operate from 2 to 100% of their nominal capacity. Furthermore, they are highly-efficient, nearly converting all consumed electricity into heat [AusIndustry, 2021].
This analysis considers two electric boiler models: one capable of delivering $7.5\frac{t}{h}$ of superheated steam at 24 bara and $310°C$, and another designed for $60\frac{t}{h}$ of supercritical steam at 80 bara and $500°C$. It is assumed both boilers achieve an efficiency of 99.6% [Bosch, 2024]. Additionally, the concept of steam-energy equivalence is applied in these models to break down heat flow into three distinct contributions, as depicted in Figure 3.11.

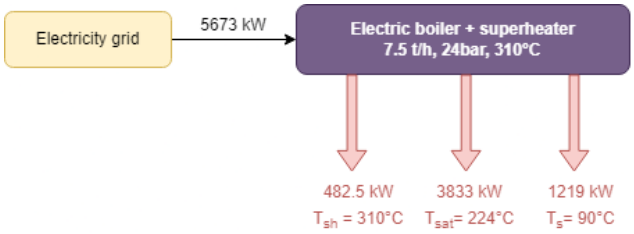

(a)) $7.5\frac{t}{h}$ of 24 bara steam superheated to 310°C

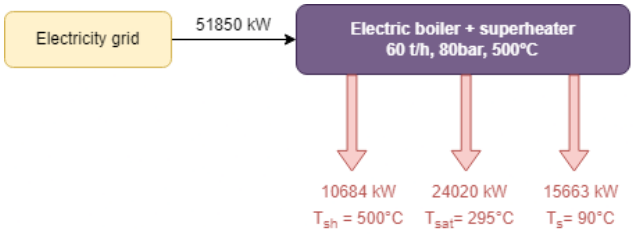

(b) 60 t/h of 80 bara, 500°C supercritical steam

Figure 3.11: Electric boiler models

The 80 bar electric boiler's capacity is bounded by $f = \{1, 2\}$. While the 24 bar electric boiler's capacity is bounded by $f = \{1, 20\}$.

3.2.8 Catalytic Methanation

Methane is a important energy carrier for the global transportation, energy, and industrial sectors. It is a fundamental component of contemporary economies due to the distribution infrastructure that is currently in place in many nations. Fossil natural gas resources provide the majority of the methane used in industrial processes. However, the discussion around the depletion of fossil fuels and climate change led to research spending on the catalytic and biological processes that produce methane (methanation) from carbon oxide-rich gases [Rönsch et al., 2016].
The methanation unit converts H_2 and CO_2 gases into SNG via a highly exothermic catalytic reaction. The pressure and temperature conditions of the reaction in the reactor are taken from [Flórez-Orrego et al., 2020].
The methanation model introduced in the superstructure is shown in Figure 3.12.

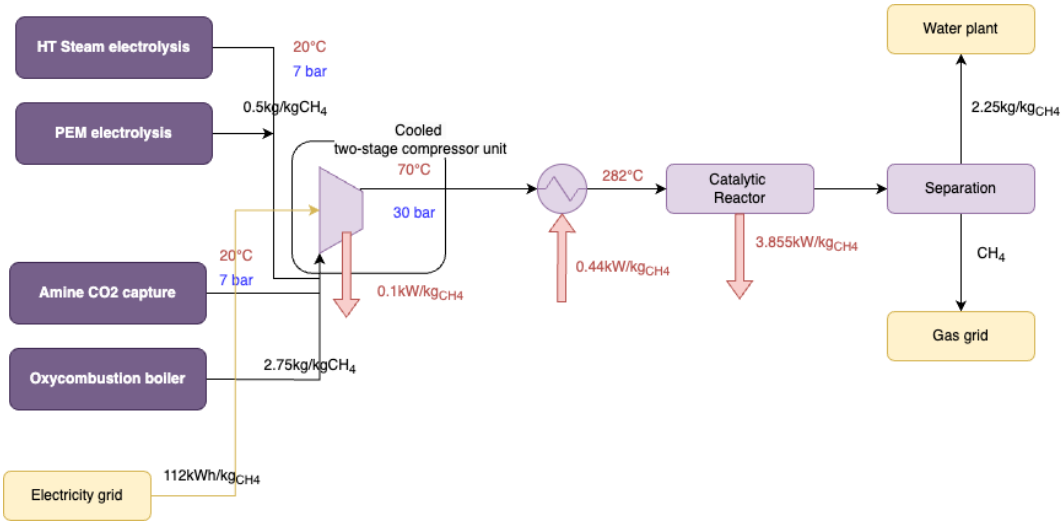

Figure 3.12: Model of the catalytic methanation unit

The economics included in the model are taken from [Baier et al., 2018] and comprise an investment cost of 300 EUR/kgCH4 for the investment cost and an operating cost of 0.005 $\frac{EUR}{kgCH4}$ produced.
The methanator's capacity is bounded by $f = \{1, 200\}$

4

Results

4.1 Industrial Utility Framework

This section describes the industrial cluster used in the optimization model. New decarbonisation units have been integrated described previously, expanding on the base case technologies developed.

Figure 4.1 presents the superstructure of the industrial cluster, illustrating the integration of base case models, decarbonization strategies, and consumer interactions. It shows the production of decarbonized fuels, specifically methanol (MeOH) and SNG, and clarifies emission trajectories by separating biogenic (considered high quality process CO_2) from fossil CO_2 emissions. The figure further maps the flow of resources such as biomass, natural gas, and water, detailing both their supply to consumer clusters and the associated returns and emissions.

4.1.1 Energy demands

Steam demands

This section presents the steam usage data utilized in the superstructure for all consumers. It details each consumer's respective steam pressure, temperature, and flowrate. Not all steam used is fully returned; therefore, the return rate (RR) of the hot condensate to the "WaterPlant" super utility is also specified.

Table 4.1: Steam Consumption Data for Cluster 1

Cluster 1: Steam demands				
Consumer	**Pressure [bara]**	$T_{superheating}$ **[°C]**	**Flowrate** $[\frac{kt}{y}]$	**RR [%]**
1	10	0	604.5	69
4 HP	15	21	57.6	80
4 LP	5.5	24	230.4	42
5	57	57	185.9	22
6 HP	15	41	41.6	84
6 LP	4	9	83.2	65

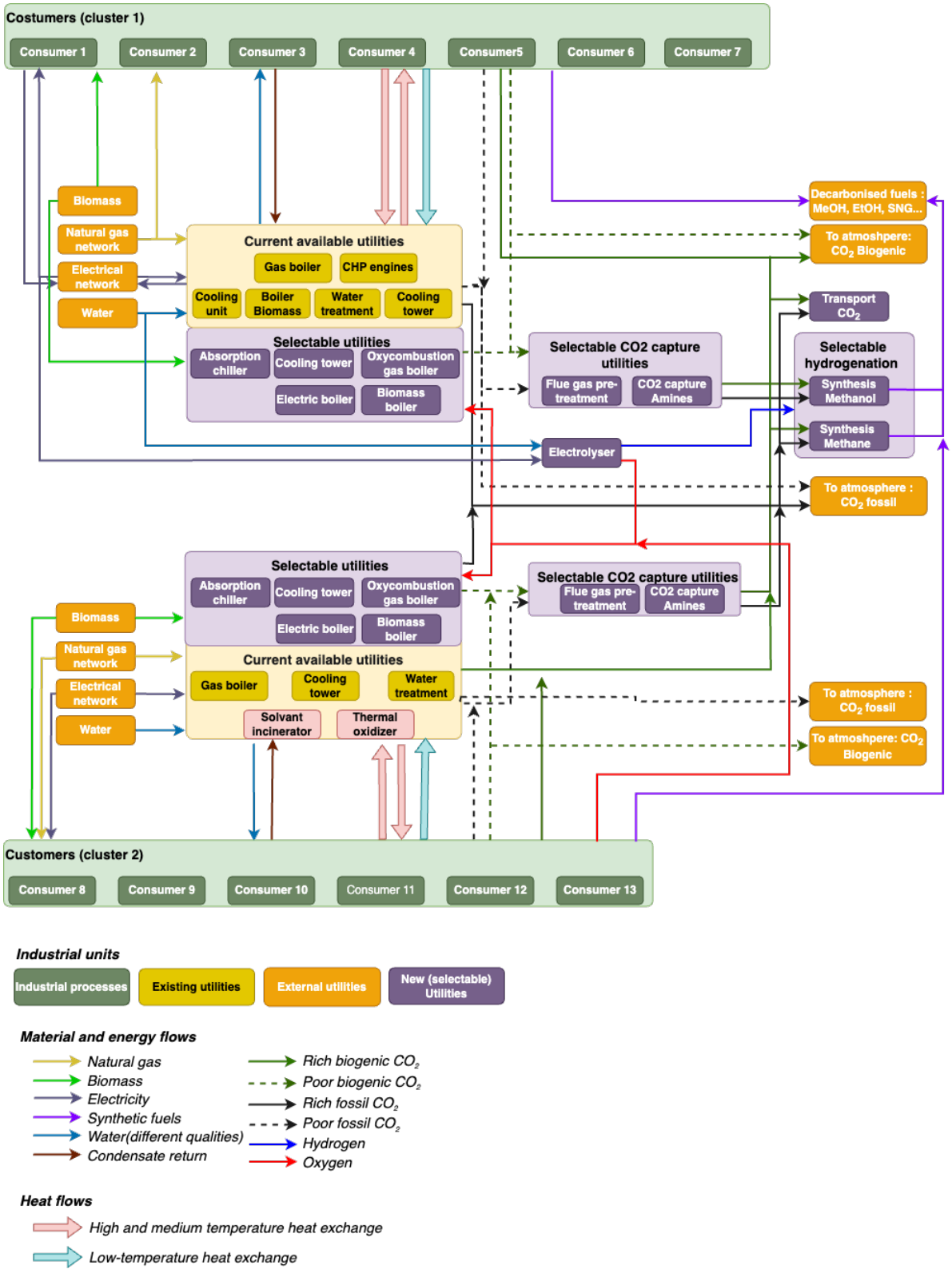

Figure 4.1: Superstructure with 2 clusters, utilities and their interconnections

Table 4.2: Steam Consumption Data for Cluster 2

Cluster 2: Steam demands				
Consumer	**Pressure [bara]**	$\Delta T_{superheating}$ **[°C]**	**Flowrate** $[\frac{kt}{y}]$	**RR [%]**
8	15	7	35.7	86
9	15	7	52.7	77
10	15	7	12.9	69
12	15	7	19.8	100

General energy demands

In addition to steam, the superstructure also accounts for the consumption of other energy carriers such as electricity and natural gas. This segment details the broader energy demands across the two clusters, illustrating the variability in consumption patterns which includes electricity, gas, and cold demand metrics.

Table 4.3: Energy Consumption Data for Cluster 1

Cluster 1: Energy demands			
Consumer	**Electricity [kW]**	**Gas [MW]**	**Cold demand [t/h]**
1	6037	23	4600
2	-	-	-
3	1952	-	-
4	4932	-	5.5
5	-	-	-
6	2283	-	-
7	1484	14	-

Table 4.4: Energy Consumption Data for Cluster 2

Cluster 2: Energy demands			
Consumer	**Electricity [kW]**	**Gas [MW]**	**Cold demand [t/h]**
8	-	-	524
9	1366	-	920
10	795	-	161
11	-	-	-
12	-	-	251
13	140	-	-

In order to meet CO_2 emissions restrictions and effectively depict the industrial site, it is necessary that various emission forms are included, including fossil and biogenic sources of CO_2 emissions.
The use of 5.75 t/h of biomass for internal combustion by Consumer 1 is important to mention. In addition to providing for internal energy demands, this biomass utilisation generates 23.58 t/h of biogenic CO_2 emissions. The amine utility can be

used to capture the 4.3 t/h of CO_2 equivalent in the flue gases that results from burning natural gas.

Consumer 2 processes 18.83 t/h of biomass for internal use, resulting in 12.35 t/h of biogenic CO_2 emissions. Similarly, Consumer 11 emits biogenic CO_2 at a rate of 2.24 t/h due to process activities.

Consumer 4 emitting 1.37 t/h of CO_2 due to process-related activities and Consumer 7 using natural gas combustion to produce 2.57 t/h of CO_2, both can utilize amine capture utility to reduce emissions.

Lastly, Consumer 13, emits highly concentrated biogenic CO_2 0.29 t/h.

It is assumed that when referring to highly concentrated CO_2, this indicates a CO_2 stream that can be compressed and utilized for valorization in processes such as methanol or methanation utilities.

The minimum temperature differences required for efficient heat exchanges, 5°C for liquid phases, 2°C for phase changes, and 10°C for gaseous streams is established for all heat streams integrated into the superstructure.

The CO_2 available in the flue gases is calculated based on the flue gas composition as provided in [Faramawy et al., 2016]. The CO_2 content is assumed to be $2.13t - eq/Nm^3$ burnt [Institute and for Sustainable Development, 2005].

4.2 Uncertainty in Energy Prices

Understanding the volatility of energy prices is crucial for accurately integrating and depicting the energy system within the RO framework. Price volatility impacts the economic feasibility and operational strategies of both the industrial system and energy system, thus it is essential to model these uncertainties precisely.

Continuous distributions are utilized to characterize the uncertainties as defined in flexible uncertainty sets. To illustrate the robust framework, this section examines the uncertainties in gas and electricity pricing.

4.2.1 Electricity Price Uncertainty

Figure 4.2 presents the distribution of electricity prices in the BELPEX spot market over the period from April 18, 2023, to April 18, 2024.

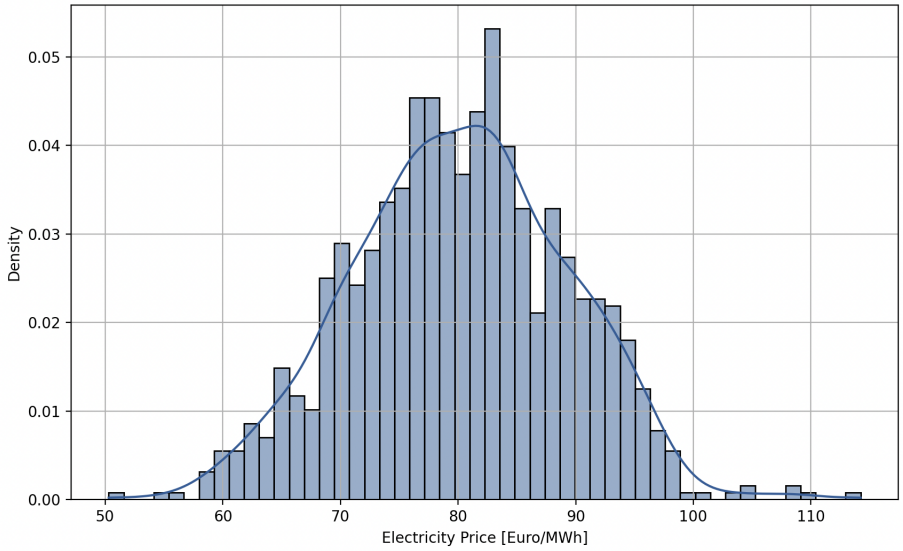

Figure 4.2: Normal Distribution of Electricity Price from BELPEX Spot market from 18/04/2023 - 18/04/2024 [Elexys NV, 2024].

For this period, the electricity price ($\tilde{c}^{+}_{elec,t}$) fluctuations can be modeled using a normal distribution, denoted as $N \simeq (80.43, 8.94)$, as also discussed in [Zhou et al., 2009, Tan and Zhong, 2022]. This standard deviation represents one-third of the uncertainty range, illustrating the variability in pricing data [Zhang et al., 2016].

4.2.2 Gas Price Uncertainty

Similarly, the gas price ($\tilde{c}^{+}_{gas,t}$) is modeled using a normal distribution, denoted as $N \simeq (50.46, 15)$, reflecting typical market behaviors and fluctuations observed in studies by [Celebi et al., 2017, Berrisch and Ziel, 2022].

4.2.3 Confidence Levels and Uncertainty Sets

Understanding the confidence levels and their associated uncertainty sets is crucial for RO, particularly in energy systems where prices are highly volatile. When dealing with uncertain parameters $\tilde{c}^{+}_{elec,t}$ and $\tilde{c}^{+}_{gas,t}$, different confidence levels (95%, 90%, 85%, and 80%) can be chosen to define the bounds of these uncertainties.
Figure 4.3 illustrates the transformed intervals for these uncertainty sets under different confidence levels. The confidence levels determine the range within which the true values of the uncertain parameters are expected to lie with a specified probability.
The normal distributions defined in Section 4.2.1 and 4.2.2 allows to calculate the probability intervals for different confidence levels. For instance, a 95% confidence interval suggests that it can be 95% certain that the true electricity price will lie within the calculated bounds.
This approach is grounded in the theory of RO as explained in Section 2.2.4.1, which aims to provide solutions that remain feasible and optimal within the uncertainty

range. The geometric interpretation of the uncertainty sets in Figure 4.3 shows how these bounds change with varying confidence levels, thus impacting the bounds of the optimization model.

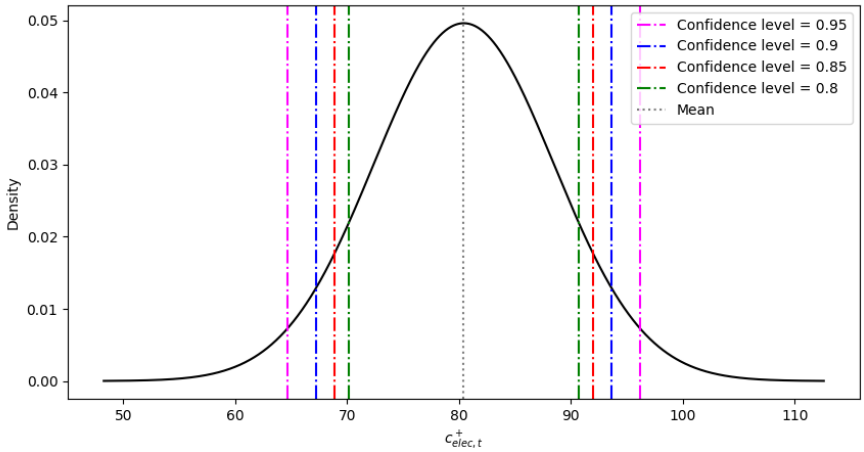

(a) Bounded uncertainties transformed from $\tilde{c}^+_{elec,t}$

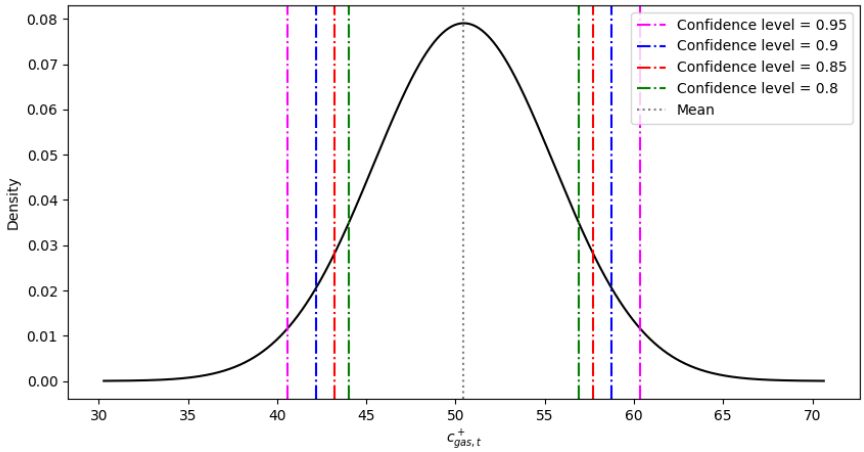

(b) Bounded uncertainties transformed from $\tilde{c}^+_{gas,t}$

Figure 4.3: Geometric interpretation for flexible uncertainty set under different confidence levels (95%, 90%, 85%, and 80%).

In practical terms, selecting a higher confidence level (e.g., 95%) results in a wider uncertainty set, offering more conservative solutions that are less sensitive to parameter variations. This conservatism comes at the cost of potentially higher operational or investment expenses. Conversely, lower confidence levels (e.g., 80%) provide narrower uncertainty sets, which may yield cost-efficient solutions but with increased risk of being less *immunized against* actual conditions.
For instance, [Ben-Tal et al., 2009, Bertsimas et al., 2011] provide comprehensive frameworks for understanding and applying RO in various contexts, emphasizing the trade-offs between solution robustness and cost-effectiveness.

4.3 Base case simulation

The base case simulation provides the reference for all CO_2 reductions, as well as for OPEX and CAPEX comparisons.

The 13 customers and the utilities that proposed in Section 4.1.1 are included in the initial simulation. This simulation is performed with the mean values for the electricity import and export prices at 80.43EUR/MWh as well as for the natural gas price at 50.46 EUR/MWh.

The system is balanced and all heat demand is satisfied by the gas boilers available to the system as well as available heat put into the heat cascade by the biomass combustion from consumer 1, the heatloads are shown in the Grand-Composite Curves (GCC) for both clusters in Figure 4.4 and Figure 4.5, cluster 1 uses a gas boiler of 71.7MW in size, cluster 2 uses a gas boiler of 47.7MW. The emissions for the base case equal to 547909.3 $\frac{t}{y}$ or 65 t/h. Figure 4.6 displays the emission fluxes with their corresponding contributions in t/h. The simulation yields an annual operating cost (OPEX) of 71.5 million EUR with a CAPEX of 0 EUR since there is no constraint on CO_2 emissions.

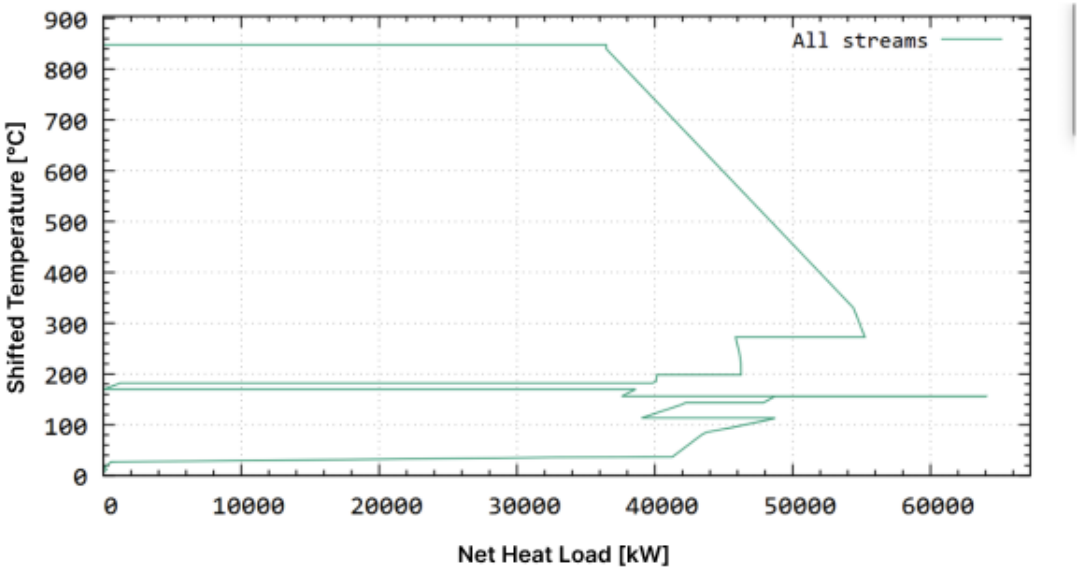

Figure 4.4: Grand Composite Curve for cluster 1 for all streams drawn with $\Delta T = 5°C$.

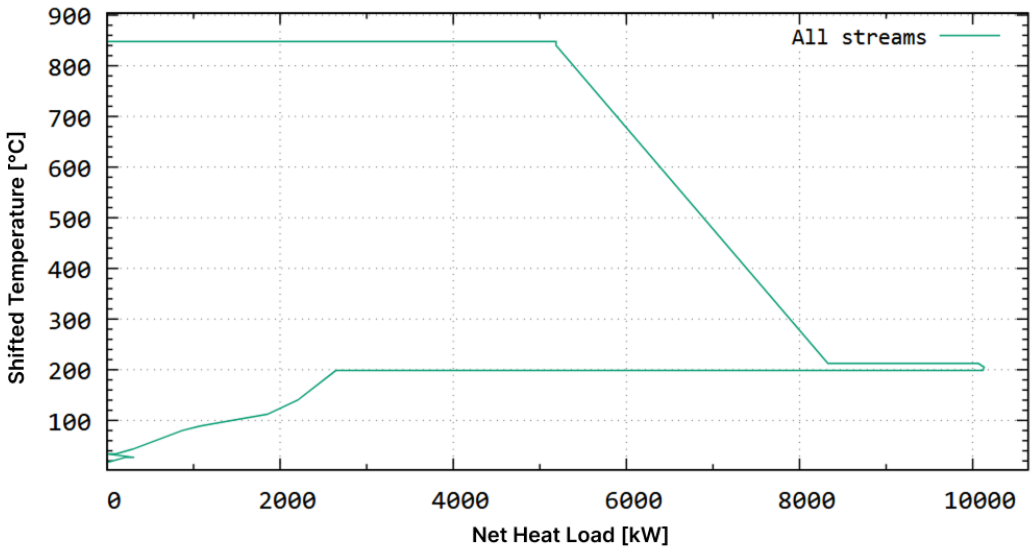

Figure 4.5: Grand Composite Curve for cluster 2 for all streams drawn with $\Delta T = 5°C$.

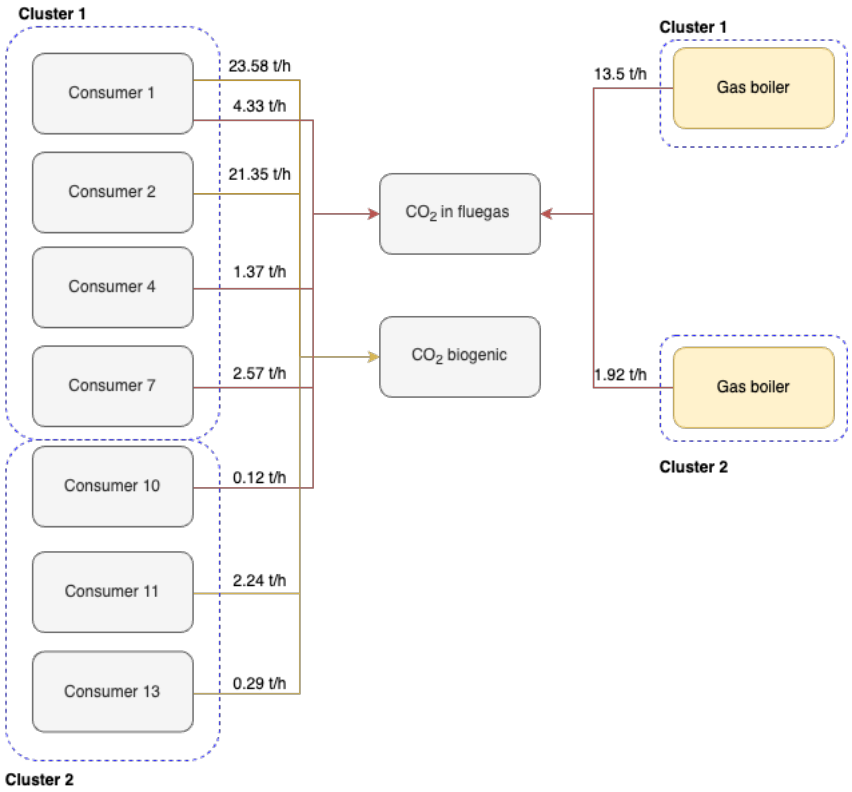

Figure 4.6: CO_2 balance base case

Figure 4.6 shows the CO_2 streams per hour in the cluster, it is important to emphisize for the sake of completeness that some consumers directly emit a stream of high quality (biogenic) CO_2 which can be directly compressed and either used or exported.

Based on an initial review of the GCCs from the base case simulations, it appears that both a Rankine cycle and a heat pump could be employed to further optimize the site. However, due to the significant impact these technologies can have on internal process configurations, they have not been developed within the scope of this thesis. For an illustration of a Rankine cycle implementation within Cluster 1, please refer to Appendix B.

4.4 Simulations Subject to CO_2 constraints

The simulations, constrained by the CO_2 limitation as detailed in Equation 2.14, explore the impact of CO_2 reduction scenarios. The scenarios operates under a constraint that progressively reduces CO_2 emissions in 10% increments, culminating in a maximum reduction of 80% relative to the baseline emissions specified in Section 4.3. It is important to note that in this work there is no difference between biogenic and fossil CO_2 in terms of CO_2 emissions, both of these forms have the same weight on the emissions of the clusters, in reality the capture of biogenic CO_2 emissions would be considered negative emissions. This requires either capturing the CO_2 or employing alternative technologies to meet these constraints. Notably, captured CO_2 must be valorized, potentially through processes like methanation or methanol production, which also necessitate additional resources such as hydrogen (H_2).
To assess the implications on the energy system, the following scenarios are investigated for their configuration and feasibility:

1. Captured pure CO_2 may be sequestrated at a cost of 100 EUR/t[1], without a cap on the quantity. The export of other resources, such as H_2 and O_2, is not permitted.
2. Captured pure CO_2 is limited to sequestration rates of 20 t/h for Cluster 1 and 5 t/h for Cluster 2, priced at 100 $\frac{EUR}{t}$. The export of other resources, such as H_2 and O_2, is not permitted.
3. All captured pure CO_2 must be utilized internally; the export of other resources such as H_2 and O_2 is also prohibited.
4. All captured pure CO_2 must be utilized internally; however, the export of other resources such as H_2 and O_2 is permitted.

Both O_2 and H_2 are assigned a selling value of zero in external markets to avoid oversizing either electrolysers or the ASU. This approach integrates the external energy system in a simplified manner, acknowledging that these clusters will not exclusively operate using internally produced resources. It is also important to note that methanol export is not constrained, as it could be utilized as fuel within the industrial cluster or exported. Additionally, no technologies using methanol are included in the current scope of the analysis.
In the scenarios outlined previously, both the original model and its robust counterpart will be analyzed comprehensively. The original model is executed using the average values for gas and electricity prices, as specified in Section 4.2. This process begins with the application of mean values in the original model, followed by

[1]This is a generically considered price, just to investigate the impact of carbon price setting and has no connection to EU ETS.

the generation of the robust counterpart. Subsequently, a detailed examination of CAPEX, TOTEX, and designated KPIs for each scenario is conducted. These KPIs include the total electricity and gas consumption of the site, the volume of MeOH sold, the quantity of SNG produced, and the cost of CO_2 avoidance, as calculated in Equation 4.1 and referenced from [Roussanaly, 2019].

$$\text{CO}_2 \text{ avoidance cost} = \frac{\text{Annualised investment CCS} + \text{Annual operating cost CCS}}{\text{Annual amount of CO}_2 \text{ emissions avoided}} \tag{4.1}$$

Scenario 1: Unlimited CO_2 sequestration at 100 EUR/t

The results for Scenario 1 are shown below, Figure 4.7 shows the CAPEX accros different CO_2 reductions for both the robust counterpart model and the original. While Table 4.6 and Table 4.5 show the most important KPIs accros the CO_2 reductions.

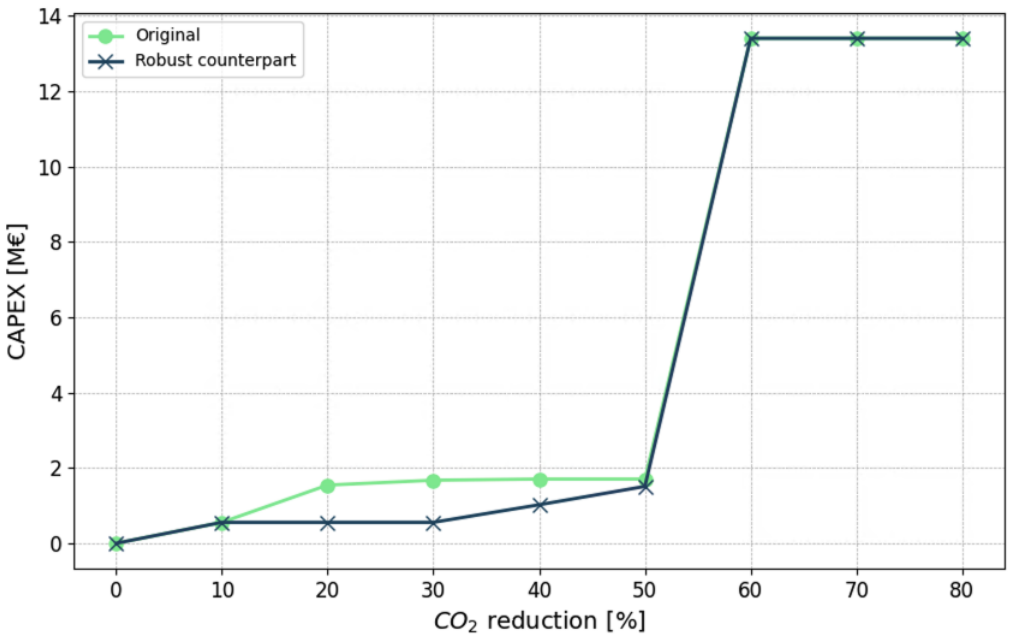

Figure 4.7: Scenario 1: CAPEX accros different CO_2 reduction constraints in %.

At a 10% reduction, both the robust and original models invest in a 25-bar electric boiler with a multiplier of $f_{\max} = 2.665$ in Cluster 2 to partially replace the gas boiler and achieve the required reduction. However, at a 20% reduction, the models diverge significantly. The original model also invests in an 80-bar electric boiler in Cluster 1, with a $f_{\max} = 1.08$, while the robust counterpart does not. Instead, the robust model opts to valorize high-quality biogenic CO_2 sourced from Consumer 11 (internally captured CO_2) and Consumer 2 (biogenic CO_2 from process), exporting this CO_2 and absorbing the associated exporting costs. This decision reflects a strategic balance between the fixed CO_2 exportation price and the internal system configuration. As a result, the original model's electricity consumption in the cluster

Table 4.5: KPIs scenario 1 for original model

CO_2 Red. [%]	Elec. [kWh]	Gas [MWh]	MeOH Exp. [t/h]	SNG [MWh]
-0	34842.0	126.2	0	0
-10	52005.0	75.9	0	0.0
-20	103766.5	19.5	0	0.0
-30	118187.4	7.0	0	0.0
-40	121068.5	4.0	0	0.0
-50	121068.5	4.0	0	0.0
-60	64998.9	71.2	0	0.0
-70	64998.9	71.2	0	0.0
-80	64998.9	71.2	0	0.0

Table 4.6: KPIs scenario 1 for robust model

CO_2 Red. [%]	Elec. [kWh]	Gas [MWh]	MeOH Exp. [t/h]	SNG [MWh]
-0	34841.0	126.2	0	0
-10	52005.0	75.9	0	0.0
-20	52005.0	75.9	0	0.0
-30	52005.0	75.9	0	0.0
-40	64443.9	63.0	0	0.0
-50	102888.0	22.9	0	0.0
-60	64998.9	71.2	0	0.0
-70	64998.9	71.2	0	0.0
-80	64998.9	71.2	0	0.0

increases by 50% due to steam production in electric boilers, whereas the robust model's electricity consumption remains unchanged.

At a 30% reduction, the original model increases the size of the 80-bar electric boiler to $f_{\max} = 1.3$ and continues valorizing 3.9 t/h of high-quality biogenic CO_2 for export. Conversely, the robust model, without an increase in CAPEX, raises its high-quality biogenic CO_2 exportation to 6.3 t/h, a 37% increase from the previous reduction increment.

At a 40% reduction, the original model further increases the 80-bar electric boiler in Cluster 1 to $f_{\max} = 1.35$, resulting in higher CAPEX and increasing the CO_2 export rate from 3.9 t/h to 9.58 t/h. Meanwhile, the robust model increases its CO_2 export to 20.7 t/h.

At a 50% reduction constraint, the original model further increases CO_2 export to 15.8 t/h. The robust model, having maximized the exportation of available high-concentrated (biogenic) CO_2, must now invest in the 80-bar electric boiler with $f_{\max} = 1$ in Cluster 1. A clear trend emerges: the original model shifts from gas to electric consumption, as evidenced by a steady increase in electrical consumption and a corresponding decline in gas consumption shown in Table 4.5). Conversely, the robust model increases its OPEX by absorbing the cost of CO_2 exportation, driven by worst-case prices for gas and electricity within the uncertainty set, guiding decision-making at this threshold.

At a 60% reduction, both the original and robust models adopt a completely different structure. They abandon the selection of electric boilers in Cluster 1 and instead invest in flue gas pretreatment and Amine capture for the flue gases of Consumer 1, the gas boiler in Cluster 1, and the biomass boiler in the base case in Cluster 1, capturing a total of 29.61 t/h of CO_2. Cluster 2 continues to use the 25-bar electric boiler with $f_{\max} = 2.66$. Consequently, as shown in Table 4.5 and Table **??**, electricity consumption decreases while gas consumption increases compared to the previous increment. All captured CO_2 is exported to the market, along with 3.91 t/h of high-quality CO_2 from cluster 1.
The convergence of both models to the same configuration at this stage is due to the optimization problem becoming highly constrained and energy price flexibility, sensitivity doesn't take the upperhand anymore. Feasibility can only be achieved in certain configurations, which, in this case, is the only viable option under both mean and robust or *worst-case* pricing scenarios.
Beyond this point, no differences in CAPEX are observed between the original and robust models from 70% to 80% reduction. The captured CO_2 and high-quality (biogenic) CO_2 are exported to the market. At 70%, the captured CO_2 accounts for 29.61 t/h, and the high-quality (biogenic) CO_2 for 10.17 t/h. At 80%, the amount of captured CO_2 remains at 29.61 t/h, while the export of (biogenic) CO_2 increases to 16.42 t/h.
At first instance the higher CAPEX in the original might seem counterintuitive, but this investigation purely looks at CAPEX and not TOTEX wich is shown in Figure

4.11 and looked at in more depth in Section 4.5.

Scenario 2: Limited CO_2 sequestration for Clusters 1 and 2 at 100 EUR/t

Scenario 2 imposes constraints on CO_2 exportation, necessitating an internal balance of other resource vectors within the system. This limitation impacts the scalability and utilization of resources and thus directly constraints the feasibility of decarbonisation.
Similar to Scenario 1, both the original and robust models adopt comparable configurations. Specifically, the robust model opts to export CO_2, while the original model invests in electric boilers to mitigate CO_2 emissions. Up to a 50% reduction, the outcomes are analogous to those observed in Scenario 1. However, beyond the 50% reduction threshold, the models must find methods to valorize CO_2 within the industrial cluster. Additionally, other resource vectors, such as H_2 and O_2, need to be internally valorized.
To achieve this, both models implement the following configuration: flue gas pretreatment for Consumer 2, the biomass boiler, and the gas boiler with capture rates of 8.4 t/h, 12.9 t/h, and 3.5 t/h, respectively, directed to the amine capture plant with $f_{\max} = 0.87$. The captured CO_2 is then valorized by activating the methanol plant with a multiplier of 0.28. To supply H_2 for methanol synthesis, a PEM electrolysis electrolyzer is chosen, operating at $f_{\max} = 40.5$. The O_2 produced by the electrolyzer is utilized in an oxy-combustion boiler, which operates at $f_{\max} = 21.1$. Additionally, a 25-bar electric boiler in Cluster 1 is implemented with a multiplier of 5.08, and Cluster 2 invests in a 25-bar electric boiler with $f_{\max} = 1.96$.

At a 70% reduction, the amine capture configuration remains unchanged, while the capacity of the oxy-combustion boiler increases to $f_{\max} = 48.7$. The electrolyzer capacity also increases to $f_{\max} = 93.35$ to support the methanol plant, which operates at $f_{\max} = 0.65$.

At an 80% reduction, the amine capture configuration remains the same, while the methanol production and the electrolyzer capacity are scaled up to $f_{\max} = 1.54$ and 220.77, respectively. The capacity of the oxy-combustion boiler also increases to $f_{\max} = 115.28$.

Table 4.7: KPIs scenario 2 for original model

CO_2 Red. [%]	Elec. [kWh]	Gas [MWh]	MeOH Exp [t/h]	SNG [MWh]
-0	34842.0	126.2	0.0	0
-10	52005.0	75.9	0.0	0.0
-20	103766.5	19.5	0.0	0.0
-30	118187.4	7.0	0.0	0.0
-40	121068.5	4.0	0.0	0.0
-50	121068.5	4.0	0.0	0.0
-60	132652.4	47.8	3.6	0.0
-70	194410.4	47.3	8.3	0.0
-80	299617.6	97.5	19.5	0.0

Table 4.8: KPIs scenario 2 for robust model

CO_2 Red. [%]	Elec. [kWh]	Gas [MWh]	MeOH Exp [t/h]	SNG [MWh]
-0	34842.0	126.3	0.0	0.0
-10	52005.0	75.9	0.0	0.0
-20	52005.0	75.9	0.0	0.0
-30	52005.0	75.9	0.0	0.0
-40	64443.9	63.1	0.0	0.0
-50	102888.0	22.9	0.0	0.0
-60	132652.4	47.8	3.6	0.0
-70	194410.4	47.3	8.3	0.0
-80	299617.6	97.5	19.5	0.0

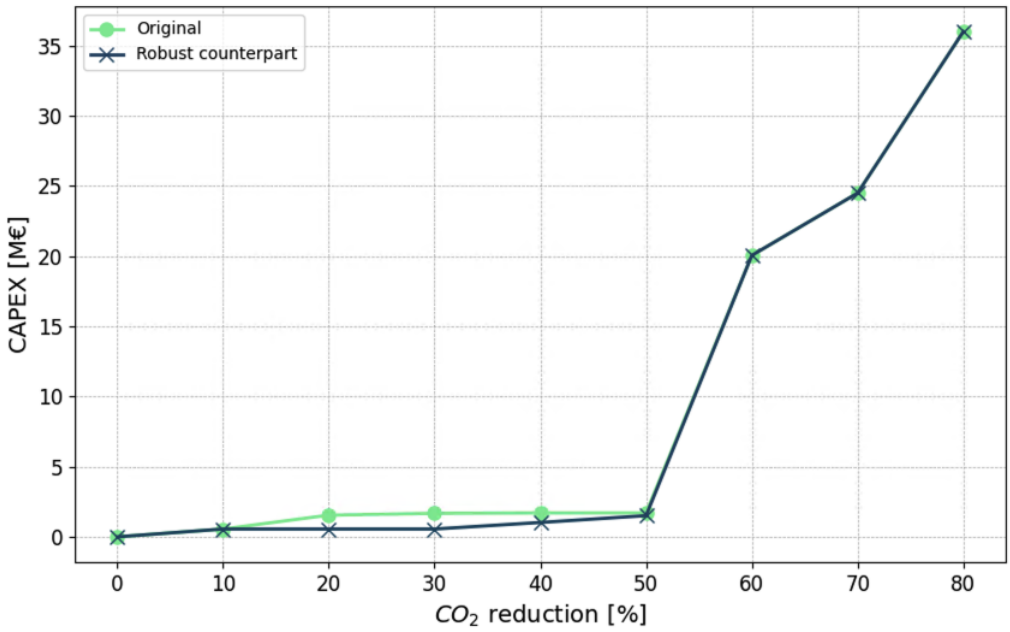

Figure 4.8: Scenario 2: CAPEX accros different CO_2 reduction constraints in %.

Scenario 3: Mandatory Internal Utilization of CO_2 (No Exports)

In terms of resource flexibility, Scenario 3 represents the most constrained condition, as all resources, including CO_2, must be utilized internally. This restriction eliminates the visibility of energy price sensitivity within this configuration. Consequently, the model becomes highly constrained, and after a 50% reduction, the optimization model becomes infeasible. No significant differences between the robust and the original model are observed in this scenario.

As previously observed, for 10% and 20% reductions, the model chooses to invest in electric boilers operating at 25 bar for both cluster 1 and cluster 2, with $f_{\max}$ values of 4.01 and 2.66, respectively.

At the point of a 30% reduction, the model selects a configuration that includes flue gas treatment for the gas and biomass boiler in cluster 1, as well as the methanol plant, the PEM electrolyzer, and the oxyboiler. The oxyboiler has a multiplier of $f_{\max} = 124.2$, absorbing all of the CO_2 produced by the electrolyzer to maintain system balance. The methanol plant operates with a multiplier of $f_{\max} = 1.54$, utilizing CO_2 for internal valorization and the H_2 produced by the electrolyzer at an $f_{\max} = 62.3$.

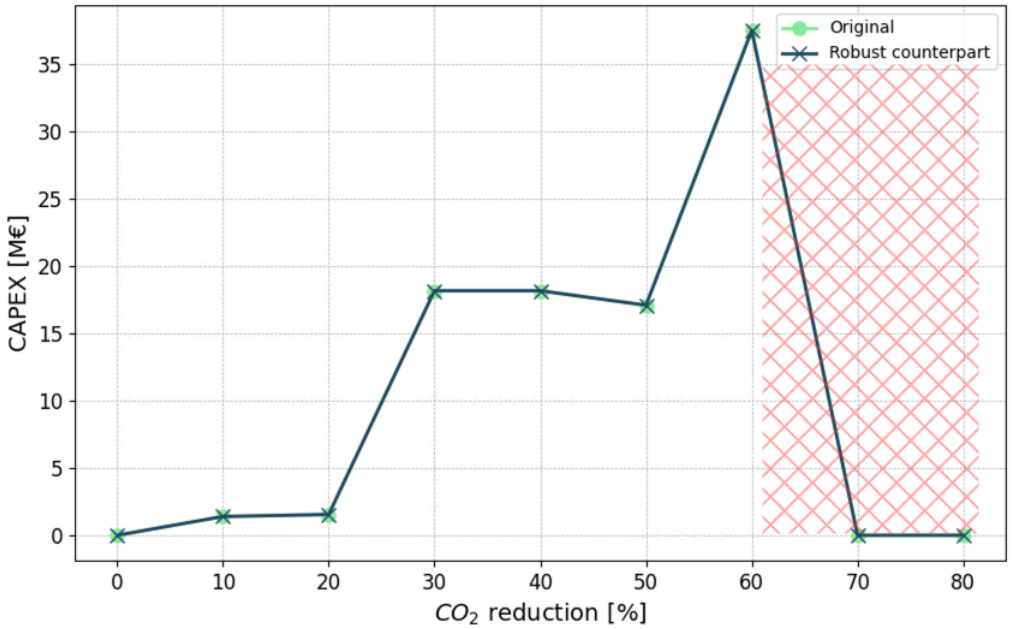

Figure 4.9: Scenario 3: CAPEX accros different CO_2 reduction constraints in %.

Table 4.9: KPIs scenario 3 for both original and robust models

Run	Elec. [kWh]	Gas [MWh]	MeOH Exp [t/h]	SNG [MWh]
-0	34842.0	126.3	0.0	0.0
-20	71955.2	52.8	0.0	0.0
-30	103766.5	19.5	0.0	0.0
-40	68013.0	104.5	19.5	222.6
-50	67420.7	97.8	19.5	222.6
-60	85958.9	158.1	32.2	222.6
-70			$\emptyset$	
-80			$\emptyset$	

Interestingly, due to the highly constrained nature of the system, at a 30% reduction, the CO_2 reduction constraint is already exceeded by 11.5%, indicating that this is the only viable configuration at this point. Consequently, there is no difference between the 30% and 40% reduction scenarios, as the configuration for a 30% reduction already meets the requirements for a 40% reduction. This further underscores the inflexibility and stringent nature of the system under these constraints.

At a 50% reduction, the CAPEX decreases slightly due to a configuration that is more expensive to operate but lower in total investment cost. The configuration changes from using the amine capture system to using only the available pure CO_2, increasing both the capacities of the SOEC electrolyzer and the oxyboiler to valorize the CO_2 together with the methanol plant. The oxyboiler has $f_{\max} = 147.74$ while the SOEC electrolyzer has $f_{\max} = 0.1$. Additionally, 23.58 t/h from Consumer 1 and 2.24 t/h from Consumer 11 are utilized.

At a 60% reduction, the configuration combines the amine capture system with a multiplier of 0.3 and the methanol plant at a multiplier of 3.5. The oxyboiler has $f_{\max} = 200$, and the SOEC electrolyzer has $f_{\max} = 102.6$. At this point, all pure CO_2 export from the consumers and flue gas treatment is needed to achieve the required reduction. This scenario requires significantly higher investments due to the constraint of internal valorization of all resources.
Internally balancing the system is particularly challenging, as various technologies with their own bounds ($f_{\min}$ and $f_{\max}$) must perfectly match consumption and demand. In many cases, such as with H_2, CO_2, and CO_2 in this scenario, achieving this balance becomes infeasible, in this case the oxyboiler reaches it's f_{max} at 200, not being able to valorize enough O_2 to balance the system.

Scenario 4: Mandatory Internal Utilization of CO_2 with Allowed H_2 and O_2 Exports

Scenario 4 mandates the valorization of all captured and available CO_2 within the industrial cluster, while permitting the export of other resource vectors. The original model invests in electricity usage to provide steam, installing a 25-bar electric boiler with $f_{\max} = 4$ in Cluster 1, and another 25-bar electric boiler with $f_{\max} = 2.66$ in Cluster 2.

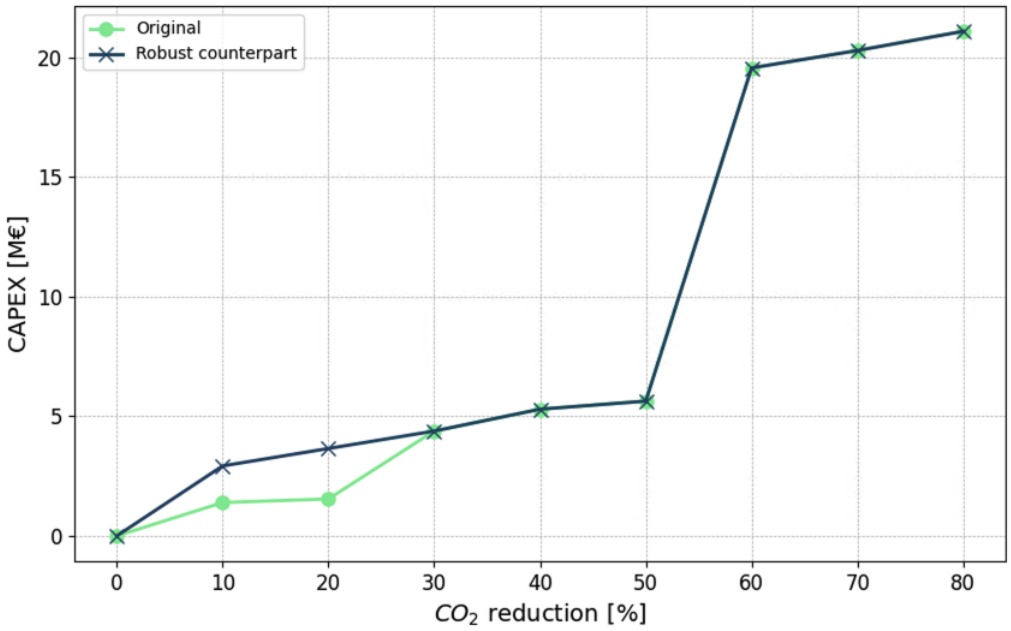

Figure 4.10: Scenario 4: CAPEX accros different CO_2 reduction constraints in %.

In contrast, the robust model prioritizes the combination of the methanol plant and the SOEC electrolyzer from the outset to valorize CO_2, rather than increasing electrical consumption. This approach effectively utilizes CO_2 from Consumer 1 and Consumer 11 at rates of 23.58 t/h and 2.42 t/h, respectively. At a 30% reduction, the original model replaces the 25-bar boiler in Cluster 1 with an 80-bar boiler. The investment cost remains unchanged from the previous reduction level, but the new configuration reduces emissions from the gas boiler needed to provide high-pressure steam.

At this stage, the robust model incrementally increases the combination of methanol production and SOEC hydrogen production to valorize the total CO_2 available internally, achieving a rate of 45 t/h. The methanol plant operates at $f_{\max} = 1.01$, and the SOEC at $f_{\max} = 35.44$. By the 30% reduction mark, both models converge on the SOEC-methanol plant configuration until a 50% reduction is achieved.

At the 50% reduction threshold, both models combine SOEC, methanol production, and electric boilers at 80 bar in Cluster 1 with $f_{\max} = 1$, and 25-bar electric boilers in Cluster 2 with $f_{\max} = 2.66$. Beyond this point, the models replace the electric boilers with investments in oxyboilers.

At a 60% reduction, both models invest in amine carbon capture with a multiplier of 0.3, combined with the methanol plant at a multiplier of 3.5, and an oxyboiler at $f_{\max} = 164.9$ and an electrolyser at $f_{\max} = 82.7$. Beyond this point, the oxyboiler capacity does not increase further as the additional O_2 produced can be exported. This balance between the valorization of O_2 and the heat input into the system via the oxyboiler is maintained.
After the 60% reduction, the configuration scales linearly, as illustrated in Figure 4.10. The analysis indicates that the most challenging constraint in this configuration is the valorization of O_2 within the system. This linear scaling approach appears optimal only if the O_2 can be exported. Ultimately, the amine capture scales up to $f_{\max} = 0.88$, the methanol plant reaches its maximum $f_{\max} = 5$, and the SOEC achieves $f_{\max} = 285$

Table 4.10: KPIs for Scenario 4 for both original and robust models

Run	Elec. [kWh]	Gas [MWh]	MeOH Exp [t/h]	SNG [MWh]
-0	34842.0	126.3	0.0	0.0
-10	71955.2	52.8	0.0	0.0
-20	103766.5	19.5	0.0	0.0
-30	69003.6	65.3	11.1	0.0
-40	85320.3	50.1	13.7	0.0
-50	122470.1	10.8	12.8	0.0
-60	80581.0	76.0	25.9	0.0
-70	86897.5	72.0	32.1	0.0
-80	98394.4	59.1	44.9	0.0

Table 4.11: KPIs for Scenario 4 for original model

Run	Elec. [kWh]	Gas [MWh]	MeOH Exp [t/h]	SNG [MWh]
-0	34842.0	126.3	0.0	0.0
-10	56379.0	74.0	3.6	0.0
-20	62690.5	69.2	7.0	0.0
-30	69004.0	66.0	12.0	0.0
-40	85320.3	50.1	13.7	0.0
-50	122470.1	10.8	12.8	0.0
-60	80581.0	76.0	25.9	0.0
-70	86897.5	72.0	32.1	0.0
-80	98394.4	59.1	44.9	0.0

4.5 General Observations

When the industrial cluster is capable of exchanging resources externally, the model demonstrates greater flexibility. This reliance on external resources alleviates certain limitations but introduces a dependency on external systems. Exploring the feasibility of achieving decarbonization by utilizing all resources internally reveals that this approach significantly complicates the infrastructure within the industrial cluster and substantially increases both CAPEX and OPEX.

In the context of the robust model, it is evident that pricing uncertainty is sensitive to external market conditions up to a certain threshold. Beyond this point, the model is constrained by the limited number of available technologies and their respective combinations needed to meet the specific requirements of the scenarios.

Across all scenarios, it is apparent that small decarbonization thresholds, under 30% reduction, are best achieved using electric boilers to lower CO_2 emissions through the flue gases of the natural gas boilers. Given the specific differences with the allowances for the use of external export, the model consistently prefers valorizing CO_2 through methanol production over methanation. Methanol production is more advantageous for valorizing CO_2 due to several key factors. Firstly, methanol synthesis requires less hydrogen, needing only 3 moles of H_2 per mole of CO_2 compared to the 4 moles required for methanation [Riedel et al., 2001, Yarbaş and Ayas, 2024]. This lower hydrogen demand translates to significant energy savings since hydrogen production is a highly energy-intensive process. Additionally, methanol synthesis operates under more moderate conditions with temperatures between 200-300°C and pressures of 50-100 bar [Pérez-Fortes et al., 2016], as opposed to the higher temperatures of 250-550°C required for methanation. These milder conditions further reduce overall energy consumption. Furthermore, the exothermic nature of the methanol synthesis reaction at these moderate conditions means less energy is needed to maintain the process, compared to the higher energy inputs required to sustain the methanation reaction. Then again, the SNG produced still has to be burned internally since export is not allowed.

Notably, the results indicate that the early adoption of deep decarbonization measures, even when targeting low levels of CO_2 reduction, is a more robust decision compared to conventional approaches. This is evidenced by the robust models across different scenarios, which often prefer methanol synthesis with various configurations over direct decarbonization units such as electric boilers.

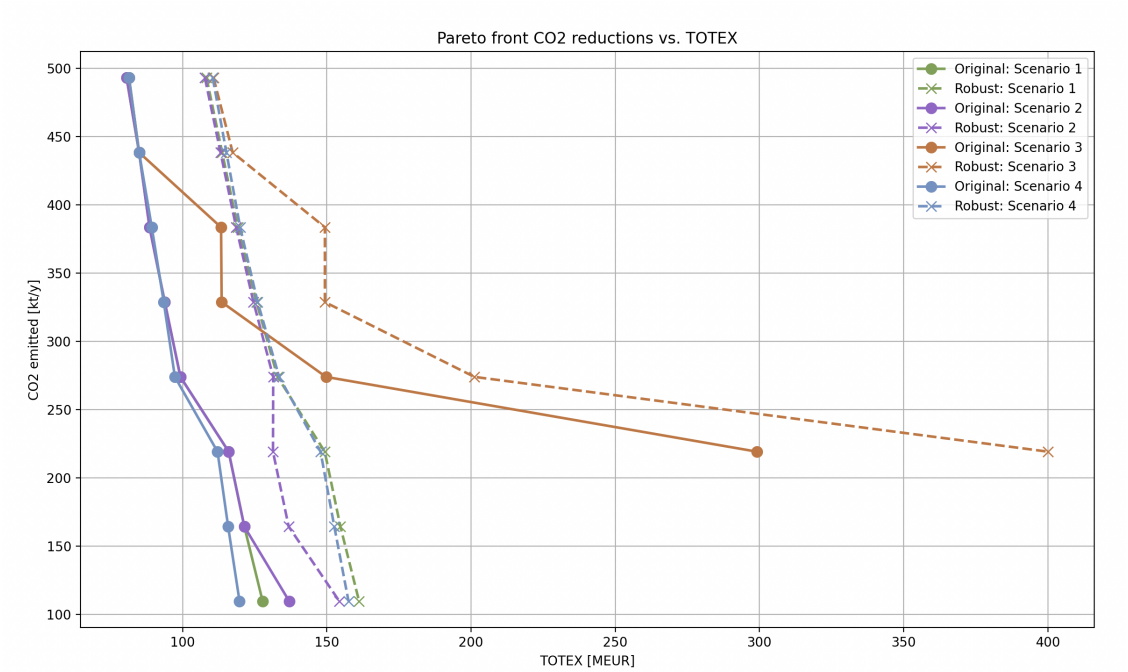

Figure 4.11: Pareto-fronts for the 4 scenarios, original and robust

The Pareto front of all scenarios, for both original and robust models, is shown in Figure 4.11. It is evident that Scenario 3 is the most constrained and thus also the most expensive configuration across all scenarios. It is also clear that the robust counterparts are always more expensive due to the worst-case scenario approach. Although CAPEX converges to the same configuration at higher CO_2 reductions, TOTEX is quite different as it takes into account OPEX and the energy prices considered in the models, since the objective function assigns equal weights to OPEX and CAPEX. This can be further illustrated by showing the solutions for the different price combinations and the respective robust model solutions within the uncertainty sets. Figure 4.12 shows TOTEX versus the different combinations of uncertainty pricing for electricity and gas with their respective probability density for a simulation at 70% CO_2 reduction for different confidence levels.
Here, it becomes clear that the robust solutions lie within the bounds and conditions predefined in the methodology. This visualization effectively demonstrates how the RO framework navigates through uncertainties in gas and electricity prices to find feasible and reliable solutions.
The figure illustrates the solution space for gas price ($\frac{EUR}{MWh}$) and electricity price ($\frac{EUR}{kWh}$) against the relative TOTEX compared to the base case in million EUR. Different confidence levels (0.95, 0.90, 0.85, and 0.80) are represented, showing the extent of the uncertainty sets considered in the optimization process. The color gradient indicates the probability density, highlighting the likelihood of different outcomes within the solution space.
This graph clearly illustrates the worst-case scenario theory, where the optimization framework ensures that the solutions remain feasible and near-optimal even in the most adverse conditions within the uncertainty sets. This approach is fundamental to RO, as it safeguards against extreme variations in input parameters [Bertsimas

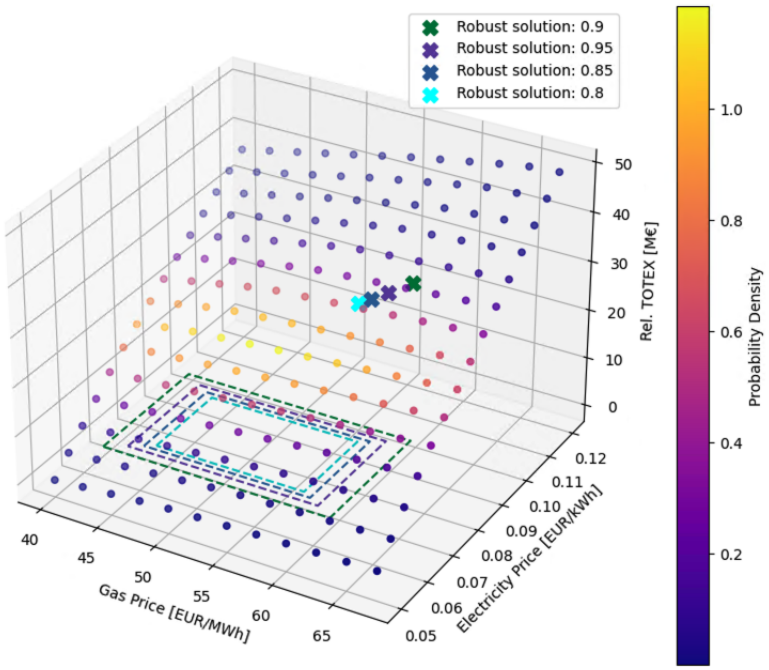

Figure 4.12: The robust solutions with their uncertainty sets in the solution space for scnario 4 at 70% CO_2 reduction.

et al., 2011, Goh and Sim, 2010].

5
Conclusion

This work successfully implemented an optimization framework for heat and resource optimization in an industrial cluster. The framework was extended to include uncertainty in pricing for electricity and gas using uncertainty set-induced robust optimization. A comprehensive overview of methodologies for accounting for uncertainty was investigated and compared to RO. To provide applicable results, an industrial cluster comprising 13 consumers was established. Additionally, decarbonization technologies were modeled and integrated into the heat and optimization model, with detailed explanations provided. Four different result scenarios were discussed, comparing the original formulation of the optimization problem with the robust formulation.

Notably, the results indicate that the early adoption of deep decarbonization measures, even when targeting low levels of CO_2 reduction, is a more robust decision compared to conventional approaches. This is evidenced by the robust models across different scenarios, which often prefer methanol synthesis with various configurations over direct decarbonization units such as electric boilers. This observation is particularly interesting and warrants further investigation to understand its implications and potential benefits fully.

While this work has successfully integrated RCs into the optimization framework, there are some inherent limitations.
This work only defines one operating point in terms of the consumers, although some industries might work at same capacity for the whole year through, defining typical operating points throughout the year might be a valuable insight. Although from a generality perspective the optimization is indeed formulated by time.
First, only one uncertainty set formulation, namely the box uncertainty set, was developed and simulated. Compared to other formulations, such as ellipsoidal or polyhedral uncertainty sets, this approach might yield conservative solutions [Ben-Tal et al., 2009, Bertsimas et al., 2011]. Future work could explore the impact of different uncertainty set formulations on the optimization outcomes.
Second, uncertainty was only considered for gas and electricity pricing. Although these are the most important energy vectors, other energy vectors and even demand distributions could also be considered. One could argue that within MILP optimization, most parameters related to energy systems should be modeled considering some distribution.
Third, the industrial cluster is limited in the decarbonization options modeled, which might limit the applicability of the results. Although this work focuses on the

methodology and the results should be considered as an example, the limited technologies might significantly affect the feasibility and configuration outcomes of the optimization results. Future research should incorporate a broader array of decarbonization technologies to provide more comprehensive insights.
In this work, only normal distributions are considered. However, in practice, continuous distributions may need to be estimated using methods such as Kernel-Based Estimation, as proposed by Zhang et al. [Zhang et al., 2016]. Despite this, the methodology described in Section 2.2.4.1 is applicable to other distribution types.
Lastly, while this work focuses on decarbonization under uncertainty, the results have been primarily investigated from a CO_2 emissions perspective. Although the water usage of respective technologies and water supply via the "WaterPlant" superutility were modeled, they were not investigated in detail. Future studies should also consider the water-energy nexus to provide a more holistic assessment of sustainability impacts

Bibliography

[Acevedo and Pistikopoulos, 1998] Acevedo, J. and Pistikopoulos, E. N. (1998). Stochastic optimization based algorithms for process synthesis under uncertainty. *Computers &; Chemical Engineering*, 22(4–5):647–671.

[AusIndustry, 2021] AusIndustry (2021). B3-oa project final report july 2021. Technical report, Austrian Government, Department of Industry, Science, Energy and Resources. Accessed: 2024-03-21.

[Baier et al., 2018] Baier, J., Schneider, G., and Heel, A. (2018). A cost estimation for co2 reduction and reuse by methanation from cement industry sources in switzerland. *Frontiers in Energy Research*, 6.

[Bell et al., 2014] Bell, I. H., Wronski, J., Quoilin, S., and Lemort, V. (2014). Chemical engineering fluid thermophysical property evaluation and the open-source thermophysical property library coolprop. *Industrial & Engineering Chemistry Research*, 53(6):2498–2508.

[Ben-Tal et al., 2009] Ben-Tal, A., El Ghaoui, L., and Nemirovski, A. (2009). *Robust Optimization*. Princeton University Press.

[Berrisch and Ziel, 2022] Berrisch, J. and Ziel, F. (2022). Distributional modeling and forecasting of natural gas prices. *Journal of Forecasting*, 41(6):1065–1086.

[Bertsimas et al., 2011] Bertsimas, D., Brown, D. B., and Caramanis, C. (2011). Theory and applications of robust optimization. *SIAM Review*, 53(3):464–501.

[Bertsimas et al., 2021] Bertsimas, D., den Hertog, D., and Pauphilet, J. (2021). Probabilistic guarantees in robust optimization. *SIAM Journal on Optimization*, 31(4):2893–2920.

[Bertsimas et al., 2015] Bertsimas, D., Dunning, I., and Lubin, M. (2015). Reformulation versus cutting-planes for robust optimization: A computational study. *Computational Management Science*, 13(2):195–217.

[Bhuiyan et al., 2022] Bhuiyan, M. A., Zhang, Q., Khare, V., Mikhaylov, A., Pinter, G., and Huang, X. (2022). Renewable energy consumption and economic growth nexus—a systematic literature review. *Frontiers in Environmental Science*, 10.

[Bosch, 2024] Bosch (2024). *Steam boiler systems from Bosch*. Accessed: 2024-03-21.

[Celebi et al., 2017] Celebi, A. D., Ensinas, A. V., Sharma, S., and Maréchal, F. (2017). Early-stage decision making approach for the selection of optimally integrated biorefinery processes. *Energy*, 137:908–916.

[Chauvel et al., 2001] Chauvel, A., Fournier, G., and Raimbault, C. (2001). *Manuel d'évaluation économique des procédés*, volume 1 of *Publications de l'Institut français du pétrole*. Ed. Technip, Paris. Bibliogr. p. [465]-478. Index.

[Chen and Zhang, 2020] Chen, Y. and Zhang, Y. (2020). Integration of renewable energy in industrial energy systems: A review. *Renewable and Sustainable Energy Reviews*, 123:109757.

[Danish Energy Agency, 2023] Danish Energy Agency (2023). Technology Data for Carbon Capture, Transport, and Storage. `https://ens.dk/sites/ens.dk/files/Analyser/technology_data_for_carbon_capture_transport_and_storage.pdf`. Accessed: 2024-03-15.

[de Saint Jean, 2014] de Saint Jean, M. (2014). *Étude énergétique et évaluation économique d'une boucle de stockage - déstockage d'énergie électrique d'origine renouvelable sur méthane de synthèse à l'aide d'un convertisseur électrochimique réversible SOEC - SOFC*. Theses, Ecole Nationale Supérieure des Mines de Paris.

[Detienne et al., 2024] Detienne, B., Lefebvre, H., Malaguti, E., and Monaci, M. (2024). Adjustable robust optimization with objective uncertainty. *European Journal of Operational Research*, 312(1):373–384.

[Diwekar, 2003] Diwekar, U. M. (2003). *Optimization Under Uncertainty*, page 145–208. Springer US.

[Elexys NV, 2024] Elexys NV (2024). Spot belpex. `https://my.elexys.be/MarketInformation/SpotBelpex.aspx`. Accessed: 2024-04-19.

[Enapter AG, 2023] Enapter AG (2023). AEM Nexus 1000 Electrolyser Datasheet. `https://handbook.enapter.com/electrolyser/aem_nexus/downloads/Enapter_Datasheet_AEM-Nexus-1000.pdf`. Accessed: 2024-03-15.

[Energie Plus Le Site, 2024] Energie Plus Le Site (2024). Machine frigorifique à absorption et à adsorption. `https://energieplus-lesite.be/techniques/climatisation8/production-de-froid/machine-frigorifique-a-ab-adsorption/`. Accessed: 2024-03-15.

[Eurostat, 2024] Eurostat (2024). Final energy consumption in industry - detailed statistics. *Statistics Explained*. Accessed: 2024-05-18.

[Faramawy et al., 2016] Faramawy, S., Zaki, T., and Sakr, A.-E. (2016). Natural gas origin, composition, and processing: A review. *Journal of Natural Gas Science and Engineering*, 34:34–54.

[Fernández-Dacosta et al., 2019] Fernández-Dacosta, C., Shen, L., Schakel, W., Ramirez, A., and Kramer, G. J. (2019). Potential and challenges of low-carbon energy options: Comparative assessment of alternative fuels for the transport sector. *Applied Energy*, 236:590–606.

[Floudas and Grossmann, 1986] Floudas, C. A. and Grossmann, I. E. (1986). Synthesis of flexible heat exchanger networks for multiperiod operation. *Computers & amp; Chemical Engineering*, 10(2):153–168.

[Floudas and Grossmann, 1987] Floudas, C. A. and Grossmann, I. E. (1987). Automatic generation of multiperiod heat exchanger network configurations. *Computers & Chemical Engineering*, 11(2):123–142.

[Flórez-Orrego et al., 2020] Flórez-Orrego, D., Sharma, S., de Oliveira Junior, S., and Maréchal, F. (2020). Combined exergy analysis, energy integration and optimization of syngas and ammonia production plants: A cogeneration and syngas purification perspective. *Journal of Cleaner Production*, 244:118647.

[François and Irsia, 1989] François, M. and Irsia, B. (1989). Synep1: A methodology for energy integration and optimal heat exchanger network synthesis. *Computers & Chemical Engineering*, 13(4–5):603–610.

[García and Peña, 2018] García, J. and Peña, A. (2018). *Robust Optimization: Concepts and Applications*. InTech.

[Goh and Sim, 2010] Goh, J. and Sim, M. (2010). Distributionally robust optimization and its tractable approximations. *Operations Research*, 58(4-part-1):902–917.

[Guo and Huang, 2021] Guo, L. and Huang, Y. (2021). Comparative study of robust and stochastic optimization for energy systems. *Energy Conversion and Management*, 231:113853.

[He and Li, 2019] He, X. and Li, W. (2019). Scalability of optimization algorithms for large-scale energy systems. *Renewable Energy*, 138:1250–1261.

[Hoffschmidt et al., 2022] Hoffschmidt, B., Alexopoulos, S., Rau, C., Sattler, J., Anthrakidis, A., Boura, C., O'Connor, B., Chico Caminos, R., Rendón, C., and Hilger, P. (2022). 3.18 - concentrating solar power. In Letcher, T. M., editor, *Comprehensive Renewable Energy (Second Edition)*, pages 670–724. Elsevier, Oxford, second edition edition.

[Ilyina, 2017] Ilyina, A. (2017). *Combinatorial Optimization under Ellipsoidal Uncertainty*. Dissertation, Technische Universität Dortmund, Dortmund, Germany. Faculty of Mathematics.

[Institute and for Sustainable Development, 2005] Institute, W. R. and for Sustainable Development, W. B. C. (2005). The greenhouse gas protocol: The ghg protocol for project accounting. Accessed: 2024-05-18.

[International Renewable Energy Agency (IRENA), 2020] International Renewable Energy Agency (IRENA) (2020). Green hydrogen cost reduction: Scaling up electrolysers to meet the 1.5°c climate goal. Report, International Renewable Energy Agency (IRENA).

[Jenbacher, 2023a] Jenbacher (2023a). Jenbacher Type 6 J616 Gas Engines. `https://www.jenbacher.com/en/gas-engines/type-6/j616`. Accessed: 2024-04-04.

[Jenbacher, 2023b] Jenbacher (2023b). Jenbacher Type 6 J624 Gas Engines. `https://www.jenbacher.com/en/gas-engines/type-6/j624`. Accessed: 2024-04-04.

[Karimi, 2012] Karimi, M. (2012). A quick-and-dirty approach to robustness in linear optimization. Master's thesis, University of Waterloo, Waterloo, Ontario, Canada. Available from University of Waterloo Libraries.

[Kermani, 2018] Kermani, M. (2018). Methodologies for simultaneous optimization of heat, mass, and power in industrial processes. page 220.

[Kermani et al., 2019] Kermani, M., Kantor, I. D., and Maréchal, F. (2019). Optimal design of heat-integrated water allocation networks. *Energies*, 12(11):2174.

[Kermani et al., 2017] Kermani, M., Périn-Levasseur, Z., Benali, M., Savulescu, L., and Maréchal, F. (2017). A novel milp approach for simultaneous optimization of water and energy: Application to a canadian softwood kraft pulping mill. *Computers &; Chemical Engineering*, 102:238–257.

[Kermani et al., 2018] Kermani, M., Wallerand, A. S., Kantor, I. D., and Maréchal, F. (2018). Generic superstructure synthesis of organic rankine cycles for waste heat recovery in industrial processes. *Applied Energy*, 212:1203–1225.

[Kermani, Maziar, 2018] Kermani, Maziar (2018). Methodologies for simultaneous optimization of heat, mass, and power in industrial processes.

[Kumbaroğlu and Madlener, 2012] Kumbaroğlu, G. and Madlener, R. (2012). Evaluation of economically optimal retrofit investment options for energy savings in buildings. *Energy and Buildings*, 49:327–334.

[LG, 2023] LG (2023). *Catalogue: Absorption Chillers*. LG Electronics. Accessed: 2024-03-15.

[Li and Fan, 2018] Li, H. and Fan, Y. (2018). A comparative study on the robustness of energy system optimization models. *Applied Energy*, 226:1087–1099.

[Li et al., 2012] Li, Z., Tang, Q., and Floudas, C. A. (2012). A comparative theoretical and computational study on robust counterpart optimization: Ii. probabilistic guarantees on constraint satisfaction. *Industrial &; Engineering Chemistry Research*, 51(19):6769–6788.

[Liu and Zhang, 2020] Liu, Z. and Zhang, C. (2020). Scalability challenges in industrial energy system optimization. *Energy Reports*, 6:347–356.

[Maréchal and Kalitventzeff, 1998] Maréchal, F. and Kalitventzeff, B. (1998). Process integration: Selection of the optimal utility system. *Computers & Chemical Engineering*, 22:S149–S156. European Symposium on Computer Aided Process Engineering-8.

[Mian et al., 2016] Mian, A., Martelli, E., and Maréchal, F. (2016). Framework for the multiperiod sequential synthesis of heat exchanger networks with selection, design, and scheduling of multiple utilities. *Industrial & Engineering Chemistry Research*, 55(1):168–186.

[Mitra and Grossmann, 2019] Mitra, S. and Grossmann, I. E. (2019). Optimal design of distributed energy systems under uncertainty. *Computers & Chemical Engineering*, 123:67–77.

[Moazeni, 2006] Moazeni, S. (2006). Flexible robustness in linear optimization. Master's thesis, University of Waterloo, Waterloo, Ontario, Canada.

[Ning and You, 2019] Ning, C. and You, F. (2019). Optimization under uncertainty in the era of big data and deep learning: When machine learning meets mathematical programming. *Computers &; Chemical Engineering*, 125:434–448.

[Nyári, 2018] Nyári, J. (2018). Techno-economic feasibility study of a methanol plant using carbon dioxide and hydrogen. Master's thesis, KTH School of Industrial Engineering and Management.

[Panja et al., 2022] Panja, P., McPherson, B., and Deo, M. (2022). Techno-economic analysis of amine-based co2 capture technology: Hunter plant case study. *Carbon Capture Science &; Technology*, 3:100041.

[Papoulias and Grossmann, 1983] Papoulias, S. A. and Grossmann, I. E. (1983). A structural optimization approach in process synthesis—ii. *Computers & Chemical Engineering*, 7(6):707–721.

[Parekh et al., 2023] Parekh, N., Kurian, J., Patil, R., and Gautam, R. (2023). A review on techno managerial approaches to energy optimization in chemical process industries. *Front. Energy Res.*, 10.

[Pérez-Fortes et al., 2016] Pérez-Fortes, M., Schöneberger, J. C., Boulamanti, A., and Tzimas, E. (2016). Methanol synthesis using captured co2 as raw material: Techno-economic and environmental assessment. *Applied Energy*, 161:718–732.

[Riedel et al., 2001] Riedel, T., Schaub, G., Jun, K.-W., and Lee, K.-W. (2001). Kinetics of co2 hydrogenation on a k-promoted fe catalyst. *Industrial &; Engineering Chemistry Research*, 40(5):1355–1363.

[Rönsch et al., 2016] Rönsch, S., Schneider, J., Matthischke, S., Schlüter, M., Götz, M., Lefebvre, J., Prabhakaran, P., and Bajohr, S. (2016). Review on methanation – from fundamentals to current projects. *Fuel*, 166:276–296.

[Roussanaly, 2019] Roussanaly, S. (2019). Calculating co2 avoidance costs of carbon capture and storage from industry. *Carbon Management*, 10(1):105–112.

[Saha and Dally, 2022] Saha, M. and Dally, B. B. (2022). Chapter 16 - solid fuels flameless combustion. In Hosseini, S. E., editor, *Fundamentals of Low Emission Flameless Combustion and Its Applications*, pages 505–552. Academic Press.

[Salazar et al., 2013] Salazar, J., Diwekar, U., Joback, K., Berger, A. H., and Bhown, A. S. (2013). Solvent selection for post-combustion CO2 capture. *Energy Procedia*, 37:257–264.

[Shi and You, 2016] Shi, H. and You, F. (2016). *Adjustable Robust Optimization for Scheduling of Batch Processes under Uncertainty*, page 547–552. Elsevier.

[Sun et al., 2018] Sun, X., Wang, Y., and Wang, J. (2018). Robust optimization for industrial energy systems. *Energy*, 143:701–711.

[Sun and Conejo, 2021] Sun, X. A. and Conejo, A. J. (2021). *Decision Making Under Uncertainty in the Power Sector*, page 1–30. Springer International Publishing.

[Sunfire GmbH, 2023] Sunfire GmbH (2023). Sunfire HyLink SOEC Factsheet - November 2023. `https://www.sunfire.de/files/sunfire/images/content/Produkte_Technologie/factsheets/Sunfire-Factsheet-HyLink-SOEC_2023Nov.pdf`. Accessed: 2024-03-15.

[Sweeten et al., 1986] Sweeten, J. M., Korenberg, J., LePori, W. A., Annamalai, K., and Parnell, C. B. (1986). Combustion of cattle feedlot manure for energy production. *Energy in Agriculture*, 5(1):55–72.

[Tan and Zhong, 2022] Tan, J. and Zhong, Q. (2022). Electricity procurement strategies under supply disruption and price fluctuation. *Complexity*, 2022:1–13.

[Turton et al., 2018] Turton, R., Shaeiwitz, J., Bhattacharyya, D., and Whiting, W. (2018). *Analysis, Synthesis, and Design of Chemical Processes*. Prentice-Hall international series in the physical and chemical engineering sciences. Prentice Hall.

[U.S. Department of Energy, 2017] U.S. Department of Energy (2017). Absorption chillers in chp systems - doe chp technology fact sheet series. `https://www.energy.gov/eere/amo/articles/absorption-chillers-chp-systems-doe-chp-technology-fact-sheet-series-fact-sheet`. Accessed: 2024-03-27.

[Vakkilainen, 2017] Vakkilainen, E. K. (2017). 3 - boiler processes. In Vakkilainen, E. K., editor, *Steam Generation from Biomass*, pages 57–86. Butterworth-Heinemann.

[Vayanos et al., 2020] Vayanos, P., Jin, Q., and Elissaios, G. (2020). Roc++: Robust optimization in c++.

[Yarbaş and Ayas, 2024] Yarbaş, T. and Ayas, N. (2024). A detailed thermodynamic analysis of co2 hydrogenation to produce methane at low pressure. *International Journal of Hydrogen Energy*, 49:1134–1144.

[Ye et al., 2014] Ye, Y., Li, J., Li, Z., Tang, Q., Xiao, X., and Floudas, C. A. (2014). Robust optimization and stochastic programming approaches for medium-term production scheduling of a large-scale steelmaking continuous casting process under demand uncertainty. *Computers &; Chemical Engineering*, 66:165–185.

[Zauner et al., 2019] Zauner, A., Böhm, H., Rosenfeld, D. C., and Tichler, R. (2019). Innovative large-scale energy storage technologies and power-to-gas concepts after optimization. D7.7 STORE&GO 691797, European Union's Horizon 2020 research and innovation programme. Deliverable Number D7.7.

[Zhang and Li, 2017] Zhang, C. and Li, Z. (2017). Decarbonization strategies in the industrial sector: A multi-criteria decision-making approach. *Journal of Cleaner Production*, 143:120–130.

[Zhang et al., 2016] Zhang, Y., Feng, Y., and Rong, G. (2016). New robust optimization approach induced by flexible uncertainty set: Optimization under continuous uncertainty. *Industrial &; Engineering Chemistry Research*, 56(1):270–287.

[Zheng et al., 2015] Zheng, C., Liu, Z., Xiang, J., Zhang, L., Zhang, S., Luo, C., and Zhao, Y. (2015). Fundamental and technical challenges for a compatible design scheme of oxyfuel combustion technology. *Engineering*, 1.

[Zhou et al., 2009] Zhou, H., Chen, B., Han, Z., and Zhang, F. (2009). Study on probability distribution of prices in electricity market: A case study of zhejiang province, china. *Communications in Nonlinear Science and Numerical Simulation*, 14(5):2255–2265.

A

Appendix 1: RC reformulation of Equation 2.12

Let n_{unc} be the set of uncertain parameters within n_r.
If r in n_{unc}:

$$C_{op} = \sum_{t=1}^{t_t} d_{op}^{t} \times \left(\sum_{r=1}^{n_{unc}} c_{r,t}^{\gamma-1,+} \times \dot{M}_{r,t}^{+} + \Psi \times \widehat{c}_{r,t}^{max} \times u_{r,t} + \sum_{u=1}^{n_u} \left[c_u^{op,fix} \times y_{u,t} + c_u^{op,var} \times f_{u,t} \right] \right) \tag{A.1}$$

$$-u_{r,t} \leq \dot{M}_{r,t}^{+} \leq u_{r,t} \quad \forall r \in n_{unc} \tag{A.2}$$

$$\Psi = \max\{c_{r,t}^{ratio}\} \quad \forall r \in n_{unc} \tag{A.3}$$

else:

$$C_{op} = \sum_{t=1}^{t_t} d_{op}^{t} \times \left(\sum_{r=1}^{n_r} c_{r,t}^{+} \times \dot{M}_{r,t}^{+} + \sum_{u=1}^{n_u} \left[c_u^{op,fix} \times y_{u,t} + c_u^{op,var} \times f_{u,t} \right] \right) \tag{A.4}$$

Or combined: Let n_{unc} be the set of uncertain parameters within n_r.
And $n_{cert} = n_r \setminus n_{unc}$

$$\begin{aligned} C_{op} = & \sum_{t=1}^{t_t} d_{op}^{t} \times \Big(\sum_{r \in n_{unc}} c_{r,t}^{\gamma-1,+} \times \dot{M}r, t^{+} + \Psi \times \widehat{c}_{r,t}^{max} \times u_{r,t} \Big) \\ & + \sum_{t=1}^{t_t} d_{op}^{t} \Big(\sum_{u=1}^{n_u} \left[c_u^{op,fix} \times y_{u,t} + c_u^{op,var} \times f_{u,t} \right] \Big) \\ & + \sum_{t=1}^{t_t} d_{op}^{t} \times \Big(\sum_{r \in n_{cert}} c_{r,t}^{+} \times \dot{M}r, t^{+} \Big) \end{aligned} \tag{A.5}$$

$$-u_{r,t} \leq \dot{M}_{r,t}^{+} \leq u_{r,t} \quad \forall r \in n_{unc} \tag{A.6}$$

$$\Psi = \max\{c_{r,t}^{ratio}\} \quad \forall r \in n_{unc} \tag{A.7}$$

B

Example: Implementation of Ranking Cycle in Cluster 1

To illustrate the potential benefits, a Rankine cycle is implemented within Cluster 1, simulated at a 40% reduction. It should be noted that no CAPEX is considered for the installation of the Rankine cycle in this example.
The Rankine cycle superstructure as proposed in [Kermani et al., 2018] adds a steam (or an organic Rankine) cycle as a developed technology to the model.
The model adapts the branching technique proposed in [Kermani et al., 2017] to:

- Generate all intermediate superheating and desuperheating thermal streams.
- Handle non-isothermal mixing at turbine inlets.
- Generate all preheating thermal streams required to reach a saturated liquid state.

These are accomplished by defining all pressure levels as mass/resource streams with corresponding temperature and enthalpy parameters.

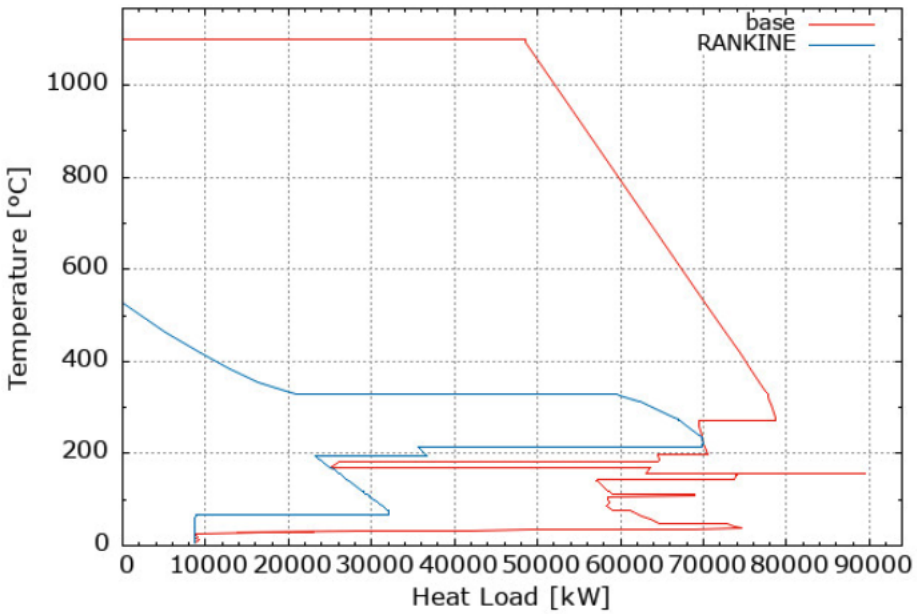

Figure B.1: Rankine Cycle with 4 pressure levels at 110, 25, 17 and 0.312 bara.

This example highlights the integration of a Rankine cycle, demonstrating the practical application of a simple Rankine Cycle generating about 9.6kW of electricity.

DEPARTMENT OF SOME SUBJECT OR TECHNOLOGY
CHALMERS UNIVERSITY OF TECHNOLOGY
Gothenburg, Sweden
www.chalmers.se

CHALMERS
UNIVERSITY OF TECHNOLOGY